
Inhomogeneous phases and color superconductivity in the NJL model

Inhomogene Phasen und Farbsupraleitung im NJL-Modell (korrigierte Version)

Master-Thesis von D. Nowakowski

Februar 2012



TECHNISCHE
UNIVERSITÄT
DARMSTADT

Institut für Kernphysik
Nuclei, Hadrons & Quarks

Inhomogeneous phases and color superconductivity in the NJL model
Inhomogene Phasen und Farbsupraleitung im NJL-Modell (korrigierte Version)

Vorgelegte Master-Thesis von D. Nowakowski

1. Gutachten: PD Dr. M. Buballa
2. Gutachten: Prof. Dr. J. Wambach

Tag der Einreichung:

Contents

1. Introduction	2
2. Color Superconductivity	3
3. Nambu–Jona-Lasinio models	4
3.1. Two-flavor Lagrangian	4
3.2. Thermodynamic potential and gap equations	6
3.3. Regularization	9
3.3.1. Three-momentum cutoff	10
3.3.2. Energetical Pauli-Villars regularization	10
3.3.3. Pauli-Villars regularization	11
3.3.4. On the regularization of temperature-dependent diverging parts in the thermodynamic potential	12
3.3.5. Parameters	14
4. Interplay of homogeneous and inhomogeneous phases	17
4.1. Homogeneous 2SC phase and homogeneous chirally broken phase	17
4.2. Homogeneous 2SC phase and inhomogeneous chirally broken phase	19
4.3. Inhomogeneous 2SC phases	20
4.3.1. Simplifications and approximations for inhomogeneous 2SC phases	25
4.3.2. Regularization and parameters	27
4.3.3. BCS phase	27
4.3.4. Fulde-Ferrell phase	29
4.3.5. General inhomogeneous phases in one dimension	33
5. Conclusion and outlook	37
A. Simplification of the effective Hamiltonian for inhomogeneous 2SC condensates	39
A.1. On the Bloch theorem and Brillouin zone	39
A.2. Derivation of the effective Hamiltonian	40

1 Introduction

The motivation to understand the smallest constituents of the world has a long lasting history; beginning with the study of the “atomos” in ancient Greece to actual knowledge of the fundamental particles of matter, called quarks, leptons and gauge bosons, people always wanted to scrutinize actual theories and get to the basic understanding behind. In the last 70 years there was an incredible progress which cumulated in a quantum field-theoretical formulation of the theory of strong interaction, called *Quantum Chromodynamics* (QCD).

This theory has very interesting features and exhibits remarkable phenomena, like confinement and asymptotic freedom, but also possesses a very rich structure in the phase diagram. The Lagrangian is given (with implicitly summing over same indices and using natural units) by

$$\mathcal{L}_{\text{QCD}} = \bar{q} \left(i\gamma^\mu D_\mu - \hat{m} \right) q - \frac{1}{4} G^{a\mu\nu} G_{\mu\nu}^a, \quad (1.1)$$

with q denoting a quark spinor with six flavors (u, d, s, c, b, t), the covariant derivative $D^\mu = \partial^\mu - ig \frac{\lambda^a}{2} A^{a\mu}$, \hat{m} the mass matrix and the gluon fields A_μ^a for color a . The gluon field strength tensor is given by

$$G_{\mu\nu}^a = \partial_\mu A_\nu^a - \partial_\nu A_\mu^a + g f^{abc} A_\mu^b A_\nu^c, \quad (1.2)$$

where g is denoting the coupling constant and f^{abc} are the structure constants of QCD, which is locally gauge symmetric under SU(3).

For high energy densities in strongly interacting matter there are two possible phase transitions: the deconfinement transition as well as the restoration of chiral symmetry. At the deconfinement transition the hadronic phase becomes a quark-gluon plasma. For high densities and low temperatures there is also a region where matter should become color-superconducting, which can be regarded as the condensation of quarks via an attractive interaction. The pairing of quarks in two flavors, namely the up and down quarks is commonly called 2SC color superconductivity, whereas the pairing of up, down and strange quarks occurs in the so called CFL phase. It is still a demanding task to explore the exact phase diagram of QCD. Experimentally there are only two directly reachable empirical points of the phase diagram at zero temperature: the vacuum state at zero chemical potential and nuclear matter-saturation density.

The main focus of this thesis is to explore the phase diagram of strongly interacting matter with respect to inhomogeneous phases in color superconductivity and study the simultaneous appearance of color-superconducting and chirally broken phases. In the first part of the thesis we analyse the interplay of homogeneous 2SC and chirally broken phases with inhomogeneous chirally broken phases. In the second part we consider 2SC condensates with a one-dimensional modulation in the order parameter and derive the corresponding phase diagram.

To circumvent the problem of the very complicated evaluation of this topic within QCD, a phenomenological Nambu–Jona-Lasinio model is used for a simplified approach. Therefore this document is organized as follows: First we introduce the concept of color superconductivity in chap. 2, present in chap. 3 Nambu–Jona-Lasinio models, review their properties and calculate thermodynamical quantities from these models. This will be used to obtain a phase diagram for chirally broken and 2SC condensates. The interplay of homogeneous 2SC and inhomogeneous chirally broken phases at different parameter sets and regularizations is studied in the following chapter 4. Beside that inhomogeneous color-superconducting condensates are considered, an extension to non-zero temperature is given and the different phase diagrams are presented. Finally we summarize our findings in chapter 5, conclude what can be learned from our results and give an outlook for remaining tasks to be done.

2 Color Superconductivity

First suggested by Collins and Perry [CP75] and by Bailin and Love [BL82] color superconductivity has not received much attention for strongly interacting quark matter for roughly twenty years. But Alford et al. [ARW98] and Rapp et al. [RSSV98] found evidence for a gap in a fermionic spectrum of the order of 100 MeV for a baryon chemical potential of around 500 MeV, which gave rise to an increased interest in color superconductivity¹.

According to the Cooper-theorem [Coo67] every system of fermions with an attractive interaction can form pairs of fermions at no free energy cost in the vicinity of the highly degenerate surface of the Fermi sphere, causing an instability in the normal state. For QCD the “Cooper-pairs” are made of quarks (as separate color carrying objects) and this is the reason why the mechanism is called *color* superconductivity, to distinguish it from the ordinary superconductivity. In general this is similar to the BCS-theory for common superconductors, where an attractive interaction between electrons is mediated by phonons, but for color superconductivity more possible condensation patterns are expected, since quarks have more degrees of freedom. The observation of bound hadrons (like “ordinary” matter) is a strong hint for the existence of color-superconducting states, because this shows, that there must be at least one attractive interaction channel in QCD. Diquarks are the primary constituents in a theory of color superconductivity and naively speaking consist of two paired quarks.

The pairing for homogeneous condensates occurs between fermions with opposite momenta $\vec{k}_1 = -\vec{k}_2$ and, if both fermions reside at the surface of the Fermi sphere, the pairing does not cost any free-energy. If the Fermi momenta of the fermions are unequal, then there is a possibility for an adaption process of the Fermi spheres to become equal and form Cooper-pairs with total momentum $\vec{k}_{\text{tot}} = 0$. Clearly this is only favored, if the energy needed for this process is compensated by the pairing energy, which sets a limit for this pairing mechanism [Clo62, Cha62] and allows for the appearance of inhomogeneous color-superconducting condensates.

One of the main consequences of color superconductivity is a gap in the single-particle spectrum, which is analogous to ordinary superconductivity and the well-known BCS-result [BCS57]

$$T_c \approx 0.57\Delta(T = 0) \tag{2.1}$$

(approximately) holds for a theory of quarks [PR99].

Color superconductivity can only be accessed in a controlled way - so far - by a weak-coupling expansion, because of asymptotic freedom of QCD. Nonetheless it was shown, that there is not only one color-superconducting phase possible, but several different phases can occur in color superconductivity [ASRS08]. Also the possible appearance of spatially varying, inhomogeneous color-superconducting condensates in the phase diagram of strongly interacting matter was studied by Alford et al. [ABR01] and others.

¹ Due to a relation between the gap and the temperature, where color superconductivity vanishes, observation of color superconductivity seemed to be more promising by the observation of gaps of the order of 100 MeV at this time, see eq. (2.1).

3 Nambu–Jona-Lasinio models

As already mentioned, the study of QCD is a very hard and tedious task and has yet not been fully solved. Lattice gauge theory simulations of QCD [KL04] have a conceptual problem for non-zero chemical potential μ , where they suffer from the fermion sign problem. This limits such studies to small, non-zero chemical potential [ABD⁺09] and renders them inapplicable for color superconductivity. Other methods also have a limited applicability. For instance perturbation theory is only valid for sufficiently large energies, while Schwinger-Dyson equations [Fis06] are computationally very hard to manage. Therefore beside the ongoing effort to solve full QCD, so called effective or phenomenological models were developed, describing the relevant degrees of freedoms and parameters of QCD while neglecting (for this region of interest) less important degrees of freedom of the full theory.

To explore various aspects of the phase diagram, there are a plethora of approaches and methods to model QCD. A sort of very popular models in the last years are the so called Nambu–Jona-Lasinio (NJL) models (first proposed in [NJL61a, NJL61b]), which are schematic phenomenological models successfully used to describe nucleon-nucleon interactions by using fermionic local point-like interactions. Nambu and Jona-Lasinio postulated in their model that a physical mass can be generated by the interaction of massless fermions in analogy to the gap of the BCS-theory of superconductors [BCS57]. Their model was used to describe strongly interacting systems, but soon after the appearance of QCD it was not attractive any more to study strongly interacting matter in such an effective model. Later it was nonetheless recognized, that it still can be used to describe non-perturbative effects of QCD in the low-energy regime and long wavelength limit while it is simpler to handle than solving full QCD. By construction the model includes mechanisms to dynamically give bare quarks an effective fermion mass and it also turns out that it respects the low-energy theorems for QCD.

As an advantage the NJL model can “be designed to share all global symmetries with QCD” [VW91], which allows to study characteristics of that complicated theory in a much more simplified version and clarify the relevant degrees of freedom. In this scheme the dynamical quark constituent mass can be understood as the spontaneous symmetry breaking of chiral symmetry, which is one of the main reason why the NJL model is often used.

One of the drawbacks of these model-types is that there are neither gluonic interactions nor confinement. This leads for example to unphysical decays of mesons in the NJL model. However, confinement is probably the least important property of QCD in the low-energy limit and can be neglected for our purposes.

Due to quadratic fermionic interactions the NJL model has coupling constants with negative energy dimension and is therefore not renormalizable, but there are several regularization schemes [Kle92] available to render divergencies finite.

3.1 Two-flavor Lagrangian

In the following we consider a two-flavor NJL-Lagrangian, review symmetries and illuminate the properties of the NJL model for this case. Here the flavor degrees of freedom are only down and up quarks. If we assume that we can include the gluon dynamics into an effective interaction so that the gluons are effectively frozen out, a typical two-flavor NJL-type isospin-symmetric Lagrangian is given for point-like quark-(anti)quark interactions in the scalar and pseudoscalar channel by

$$\mathcal{L} = \mathcal{L}_0 + \mathcal{L}_{\bar{q}q} + \mathcal{L}_{qq}, \quad (3.1)$$

where

$$\mathcal{L}_0 = \bar{\psi} (i\rlap{\not{D}} - m) \psi, \quad (3.2)$$

$$\mathcal{L}_{\bar{q}q} = G \left((\bar{\psi}\psi)^2 + (\bar{\psi}i\gamma^5 \vec{\tau}\psi)^2 \right), \quad (3.3)$$

$$\mathcal{L}_{qq} = H \sum_{A=2,5,7} (\bar{\psi}i\gamma_5 C \tau_2 \lambda_A \bar{\psi}^T) (\psi^T C i\gamma_5 \tau_2 \lambda_A \psi), \quad (3.4)$$

and ψ is a quark-field $4N_c N_f$ -spinor with N_c denoting the number of colors, N_f denotes the number of flavors, m the undressed “bare” quark mass and G is the coupling constant in the color singlet channel. The matrices γ^μ denote the conventional Dirac gamma matrices and τ^A the isospin Pauli matrices. The charge-conjugation operator C is defined as $C := i\gamma^2\gamma^0$ and H is the coupling constant for the scalar quark-quark interaction in the color anti-triplet channel.

The first part of eq. (3.3) describes scalar interactions and the second one pseudoscalar interactions in the quark-antiquark channel. The associated quark condensates are the scalar condensate $\langle \bar{\psi}\mathbb{1}\psi \rangle$ and pseudoscalar condensate $\langle \bar{\psi}i\gamma^5 \vec{\tau}\psi \rangle$.

The second part eq. (3.4) of the overall Lagrangian describes the interaction in the quark-quark channel and allows for more pairing patterns. In general the appearing diquark condensates for color superconductivity can be written in the form $\langle \psi^T \mathcal{O} \psi \rangle$, where \mathcal{O} has to be a totally antisymmetric operator. Of special interest in this condensation patterns will be the scalar 2SC condensate defined by $\langle \psi^T C \gamma_5 \tau_2 \lambda_2 \psi \rangle$, which describes the formation of condensates of red and green up and down quarks. For this choice the blue up and down quarks remain unpaired and do not participate in the 2SC quark-quark condensation. This SU(2) Lagrangian eq. (3.1) shares the important symmetries of QCD. For example in the case of isospin-symmetry (because of $m_u \approx m_d$) the SU_V(2)-symmetry holds in isospin-space. The chiral symmetry SU_R(2) \otimes SU_L(2) is defined via the invariance of the Lagrangian under transformations of the form

$$\psi_{R,L} \rightarrow \exp \left(i\theta_{R,L}^a \frac{\tau^a}{2} \right) \psi_{R,L} \quad (3.5)$$

and holds in the case of massless quarks $m = 0$ in this model. Formally the invariance of the Lagrangian is caused by the algebraic relation

$$\text{SU}_V(2) \otimes \text{SU}_A(2) \cong \text{SU}_R(2) \otimes \text{SU}_L(2) \quad (3.6)$$

where the invariance of the Lagrangian under SU_A(2)-rotations is used and

$$\text{SU}(N_f)_V : \psi \rightarrow \exp(i\theta_a^V \tau_a) \psi \quad (3.7)$$

defines the vector SU(N_f) isospin transformation. The transformation

$$\text{SU}(N_f)_A : \psi \rightarrow \exp(i\theta_a^A \gamma_5 \tau_a) \psi \quad (3.8)$$

is the so called axial vector transformation, γ_5 denotes the fifth gamma matrix, θ_a^V and θ_a^A are parameters of the transformation and τ^a denotes the generator of flavor SU(N_f). The isomorphism eq. (3.6) means that for the chiral limit the currents $j_{L,R}^\mu$ associated with the chiral symmetry can be linearly added to yield the vector current $V^{\mu,a} = j_R^{\mu,a} + j_L^{\mu,a}$ and axial-vector current $A^{\mu,a} = j_R^{\mu,a} - j_L^{\mu,a}$ which in turn also determine symmetry transformations, given on the LHS of the isomorphism.

For a sufficiently large coupling the ground state is not invariant under this transformation, which leads to spontaneous symmetry breaking in the vacuum and accounts to the appearance of chirally broken phases in our model. The order parameter of this symmetry breaking turns out to be the *chiral condensate*

of the form $\langle \bar{\psi}\psi \rangle$. In general chiral symmetry breaking in the NJL model corresponds to a different structure of the vacuum by the presence of quark-antiquark pairs, which mix left- and right-handed quarks. Therefore the chiral condensate has a non-vanishing expectation value, if the chiral symmetry is broken. This also leads to the appearance of Goldstone bosons; algebraically the spontaneously broken symmetry of the Lagrangian fulfills

$$\text{SU}_R(2) \otimes \text{SU}_L(2) \rightarrow \text{SU}_{L+R}(2), \quad (3.9)$$

which is isomorphic equivalent to $\text{SU}_V(2)$.

The 2SC condensate is a flavor singlet and it is invariant under the isospin-transformation $\text{SU}_V(2)$ and the $\text{SU}_A(2)$ -transformation. Therefore it does not break chiral symmetry. Due to the assumption of unpaired blue quarks the presence of the 2SC condensates causes the $\text{SU}_c(3)$ color symmetry to break down to a $\text{SU}_c(2)$ -symmetry.

3.2 Thermodynamic potential and gap equations

Once the thermodynamic potential for the NJL model is known, thermodynamical quantities can be extracted from it. Especially we are interested in the phase boundaries, which enable us to draw a phase diagram for strongly interacting quark matter. Since this is essential for our analysis of possible homogeneous and inhomogeneous phases, in the following the derivation of the thermodynamic potential is shown for the two-flavor NJL-Lagrangian for a homogeneous 2SC and chiral condensate.

To calculate thermodynamical quantities we consider the grand potential (or referred to as “thermodynamic potential”) per unit volume, which is given by

$$\Omega = -\frac{T}{V} \ln \mathcal{Z}, \quad (3.10)$$

where T is the temperature, \mathcal{Z} the grand canonical partition function (from now on omitting “grand canonical”) and V the unit volume.

The partition function \mathcal{Z} encodes all statistical quantities and is given by

$$\mathcal{Z} = \text{tr} \exp \left(\beta \int d^3x \mathcal{H} - \mu_i n_i \right), \quad (3.11)$$

with the μ_i 's denoting the chemical potential for the species i , $\beta = T^{-1}$, $n_i = \psi^\dagger \psi$ and \mathcal{H} is the Hamiltonian. Because we concentrate on one common chemical potential we will drop the index i for further calculations. The trace has to be understood as a functional trace running over all states of the system and the Hamiltonian is given by a Legendre transformation of the Lagrangian \mathcal{L} as $\mathcal{H} = i\psi^\dagger \dot{\psi} - \mathcal{L}$.

We constrain ourselves for further evaluations to a mean-field approximation of the thermodynamic potential Ω , where we consider scalar chiral condensates and color-superconducting condensates. For the case of homogeneous quark-antiquark condensates we assume that the only pairing between quark and antiquark happens for

$$\phi = \langle \bar{\psi}\psi \rangle. \quad (3.12)$$

For the diquark condensates we constrain our calculations to spin-0 condensates, where we focus on the most important condensate, the 2SC condensate

$$s_{22} = \langle \psi^T C \gamma_5 \tau_2 \lambda_2 \psi \rangle, \quad (3.13)$$

allowing for the pairing of up and down quarks, as already discussed.

In the mean-field approximation the values of the fields are replaced with their expectation value and fluctuations

$$(\bar{\psi}\psi) = \langle \bar{\psi}\psi \rangle + \delta(\bar{\psi}\psi)$$

and quadratical terms of the fluctuation are neglected

$$(\bar{\psi}\psi)^2 \approx \langle \bar{\psi}\psi \rangle (\bar{\psi}\psi) + (\bar{\psi}\psi) \langle \bar{\psi}\psi \rangle - \langle \bar{\psi}\psi \rangle \langle \bar{\psi}\psi \rangle,$$

which analogously also is done for the diquark condensates $\langle \psi^T \mathcal{O} \psi \rangle$.

Inserting the non-zero expectation values of diquark and chiral condensates in the Lagrangian gives

$$\begin{aligned} \mathcal{L} &= \bar{\psi} (i\partial - m) \psi + G \left(2 \langle \bar{\psi}\psi \rangle (\bar{\psi}\psi) - \langle \bar{\psi}\psi \rangle^2 \right) + \\ &\quad + H \left(\langle \bar{\psi}^T C \gamma_5 \tau_2 \lambda_2 \psi \rangle^* (\bar{\psi} C \gamma_5 \tau_2 \lambda_2 \psi) - \langle \bar{\psi}^T C \gamma_5 \tau_2 \lambda_2 \psi \rangle (\bar{\psi} \gamma_5 \tau_2 \lambda_2 C \bar{\psi}^T) - |s_{22}|^2 \right) \\ &= \bar{\psi} (i\partial - m + 2G \langle \bar{\psi}\psi \rangle) \psi - G \langle \bar{\psi}\psi \rangle^2 + H \left(s_{22}^* (\bar{\psi} C \gamma_5 \tau_2 \lambda_2 \psi) - s_{22} (\bar{\psi} \gamma_5 \tau_2 \lambda_2 C \bar{\psi}^T) - |s_{22}|^2 \right) \\ &= \bar{\psi} (i\partial - M) \psi - \frac{|M - m|^2}{4G} + \frac{1}{2} \left(\bar{\psi} \Delta \gamma_5 \tau_2 \lambda_2 C \bar{\psi}^T - \psi^T C \Delta^* \gamma_5 \tau_2 \lambda_2 \psi - \frac{2|\Delta|^2}{4H} \right). \end{aligned} \quad (3.14)$$

Here the diquark-condensate s_{22} is related to physical observables, by substituting

$$\Delta = -2Hs_{22} \quad (3.15)$$

for the so called *diquark gap* Δ . The chiral condensate ϕ is replaced by the *constituent quark mass* M

$$M = m - 2G\phi. \quad (3.16)$$

If the so called Nambu-Gor'kov formalism [Gor59, Nam60] is used the notation of the Lagrangian eq. (3.14) becomes more compact. The idea is to introduce bispinors of the form

$$\Psi = \frac{1}{\sqrt{2}} \begin{pmatrix} \psi \\ \psi^C \end{pmatrix}, \quad (3.17)$$

by assuming that ψ and $\psi^C = C\bar{\psi}^T$ are formally independent. This enables us to re-express the Lagrangian in a matrix-like form

$$\mathcal{L} + \psi^\dagger \mu \psi = \mathcal{L} + \bar{\psi} \gamma_0 \mu \psi = \bar{\Psi} S^{-1} \Psi - \mathcal{V}, \quad (3.18)$$

where additionally a chemical potential μ was added and the resulting Lagrangian is bilinear in the Nambu-Gor'kov fields. Here Ψ and $\bar{\Psi}$ are bispinor fields in Nambu-Gor'kov formalism, S^{-1} denotes the dressed inverse Nambu-Gor'kov propagator given by

$$S^{-1} = \begin{pmatrix} i\partial - M + \mu\gamma^0 & \Delta\gamma_5\tau_2\lambda_2 \\ -\Delta^*\gamma_5\tau_2\lambda_2 & -i\partial - M - \mu\gamma^0 \end{pmatrix} \quad (3.19)$$

and \mathcal{V} denotes the potential absorbing terms without any quark-field dependency. Explicitly it is given by

$$\mathcal{V} = \frac{(M - m)^2}{4G} + \frac{|\Delta|^2}{4H}. \quad (3.20)$$

Inserting this into the partition function \mathcal{Z} the thermodynamic potential reads

$$\Omega(T, \mu) = -T \sum_n \int \frac{d^3k}{(2\pi)^3} \frac{1}{2} \text{tr} \ln \left(\frac{1}{T} S^{-1}(i\omega_n, \vec{k}) \right) + \mathcal{V}, \quad (3.21)$$

where ω_n are fermionic Matsubara frequencies which arise because of the anti-periodicity in imaginary time-direction and the factor of 1/2 is present because of the artificial doubling of degrees of freedom in Nambu-Gor'kov formalism. Identifying the inverse propagator S^{-1} in momentum space with

$$S^{-1}(k^0, \vec{k}) = \gamma^0 (k^0 - \mathcal{H}(\vec{k})) \quad (3.22)$$

and using the identity

$$\text{tr} \ln = \ln \det, \quad (3.23)$$

allows to evaluate the thermodynamic potential by determining the eigenenergies of the effective Hamiltonian $\mathcal{H}(\vec{k})$. For homogeneous condensates this is straight forward and one finds that they appear in pairs with opposite sign. Turning out the Matsubara sum gives in the infinite volume limit [Kap89]

$$\Omega(T, \mu) \equiv \Omega_0 + \mathcal{V} = -\frac{1}{4} \int \frac{d^3k}{(2\pi)^3} \sum_{\lambda} \left(\epsilon_{\lambda}(\vec{k}) + 2T \ln \left(1 + \exp \left(-\frac{\epsilon_{\lambda}(\vec{k})}{T} \right) \right) \right) + \mathcal{V}, \quad (3.24)$$

where ϵ_{λ} denotes the eigenvalues of \mathcal{H} . For the case of the two-flavor NJL model the eigenvalues of the Hamiltonian \mathcal{H} are given by

$$\epsilon_{\pm}(\vec{k}) = \epsilon_{\pm} = \epsilon \pm \mu \quad (3.25)$$

and

$$E_{\pm}(\vec{k}) = E_{\pm} = \sqrt{\epsilon_{\pm}^2 + |\Delta|^2} \quad (3.26)$$

for a given momentum \vec{k} , where we defined $\epsilon(\vec{k}) = \epsilon = (\vec{k}^2 + M^2)^{1/2}$ and the eigenenergies ϵ_{\pm} and E_{\pm} are 8- and 16-fold degenerate. Physically these eigenvalues correspond to the dispersion relation ϵ_{\pm} for an (anti-)particle in a chemical potential μ and the dispersion relation E_{\pm} for a particle in a superconducting state with energy gap Δ .

For inhomogeneous condensates in color superconductivity the diagonalization of the Hamiltonian is not trivial any more, because it is not diagonal in momentum-space, but it can in principle be diagonalized, because of the hermiticity of \mathcal{H} . Since this is more complicated than in the case for homogeneous phases, we will consider the formalism for inhomogeneous condensates later in detail.

At this stage it is also worth to point out that the thermodynamic potential is only determined up to a constant, which will normally be omitted in our notation. For sake of clarity we write the parameters M and Δ and possible other condensates explicitly in the dependency of the thermodynamic potential $\Omega(T, \mu) \equiv \Omega(T, \mu; M, \Delta, \dots)$, even if they are not real variables and depend on T and μ .

In general the minimization of the thermodynamic potential

$$\frac{\partial \Omega(T, \mu)}{\partial \tilde{q}} \stackrel{!}{=} 0, \quad (3.27)$$

for $\tilde{q} = (M^*, \Delta_i^*, \dots)$ containing the order parameter for each condensate, leads to a set of gap equations. These are coupled integro-differential equations, which need to be numerically solved.

For our thermodynamic potential eq. (3.24) these equations determine the gap Δ and the constituent quark mass M self-consistently:

$$\Delta = 8H \int \frac{d^3k}{(2\pi)^3} \left(\sum_{\lambda=\pm} \frac{\Delta}{E_\lambda(\vec{k})} (1 - 2n(E_\lambda(\vec{k}))) \right) \quad (3.28)$$

$$M = m + 8G \int \frac{d^3k}{(2\pi)^3} \frac{M}{\epsilon(\vec{k})} \left(\sum_{\lambda=\pm} \left(\frac{\epsilon_\lambda(\vec{k})}{E_\lambda(\vec{k})} (1 - 2n(E_\lambda(\vec{k}))) \right) + 1 - n(\epsilon_+(\vec{k})) - n(\epsilon_-(\vec{k})) \right), \quad (3.29)$$

where $n(E) := (\exp(E/T) + 1)^{-1}$ is the Fermi-Dirac distribution function.

The thermodynamic potential of the NJL model is in general divergent in the momentum integration and also the gap-equations $\partial\Omega/\partial q$ are normally divergent. Because of point-like interactions in the NJL model, renormalization techniques are not applicable within this framework. Thus there is a need for a regularization scheme to render the momentum-integration finite. For inhomogeneous phases the effect of the chosen regularization scheme is even more crucial, since a wrong choice would lead to unphysical artefacts in the theory, like the limitation of the momentum-space to very few allowed values or the vanishing of the coupling of different momenta.

This is our motivation to present in the following section different regularization methods for homogeneous, as well as for inhomogeneous phases.

Having found a suitable regularization procedure for both - homogeneous as well as inhomogeneous - condensates, we allow the different inhomogeneous and homogeneous phases to compete with each other.

3.3 Regularization

In general for NJL-like models the momentum integration is divergent. In eq. (3.24) the eigenenergies eqs. (3.25) and (3.26) of the Hamiltonian $\mathcal{H}(\vec{k})$ lead to a divergency in the momentum integration. To remove such divergencies one must define a procedure to overcome this problem, which is called *regularization scheme* and assign some values to the (vacuum) observables of the model. As a necessity the regularization scheme should not produce unphysical behavior and respect the symmetries of the model. In principle every scheme which is able to regularize the integration is suited to be applied to our model, because for a non-renormalizable model there is no unique regularization scheme. As a requirement for the regularization procedure we follow Klevansky [Kle92] and demand that this procedure should allow for the appearance of Goldstone bosons resulting from certain symmetry operations in the model and do not restrict important quantities.

For the regularization it is mostly assumed that there is no angular dependency of the momentum components, which allows to simplify the integration by using spherical coordinates. For spatially varying condensates this is in general not possible, because the assumption of homogeneity of the momentum components is not valid and one cannot assign the energy for one quasi-particle by a constant, conserved three-momentum. In the case of inhomogeneous phases different momenta are in general coupled and it turns out that a three-momentum cutoff would limit the observable physics too stringently.

In general we have to carefully choose our regularization scheme, since we are interested in generalizing our scheme from homogeneous to inhomogeneous phases and do not want to have regularization artefacts in the region of interest. In the following different regularization methods are presented and the applicability to inhomogeneous phases is reviewed.

3.3.1 Three-momentum cutoff

The most naive regularization of the momentum integration is the so called *three-momentum cutoff* [VW91, Kle92], where the basic idea is to describe only physics up to a certain momentum scale $|k| < \Lambda$. Modes with higher momentum above this scale are not included in the calculations and are “cut off”. Clearly this three-momentum cutoff violates Lorentz-invariance, because of the non-covariant cutoff of the momentum-components \vec{k} , but it is still widely used. A three-momentum cutoff regularization scheme can additionally produce unphysical artefacts for inhomogeneous phases by limiting the allowed momenta to $k_{\text{tot}} \leq 2\Lambda$ and will not be used in our calculations.

3.3.2 Energetical Pauli-Villars regularization

A very attractive Lorentz- and gauge-symmetry preserving regularization scheme was originally proposed by Pauli and Villars [PV49]. Their idea was to introduce heavy (unphysical) masses in the integral to overcome the divergent terms by adding sufficiently many counterterms.

In the case of a system with two-flavor color superconductivity and chiral symmetry breaking the original idea of Pauli-Villars is adopted for the so called *energetical Pauli-Villars regularization scheme* and regulators are inserted in the unregularized thermodynamic potential eq. (3.24) to yield finite values for the thermodynamic potential

$$\Omega(T, \mu; M, \Delta) = -\frac{1}{4} \int \frac{d^3k}{(2\pi)^3} \sum_{\lambda} \sum_{j=0}^{r_{\text{PV}}} c_j \left(E_{\lambda,j} + 2T \ln \left(1 + \exp \left(-E_{\lambda,j}/T \right) \right) \right) + \frac{|M - m|^2}{4G} + \frac{|\Delta|^2}{4H}, \quad (3.30)$$

where r_{PV} denotes the maximal number of introduced regulators. This corresponds to the substitution

$$E_{\lambda} \rightarrow \sum_j c_j E_{\lambda,j} \quad (3.31)$$

of the diverging parts in the thermodynamic potential, where the factors $c_j \in \mathbb{R}$ will be defined later. Because the unregularized temperature-dependent part of the thermodynamic potential does not show a divergency it is also possible to let this latter part in eq. (3.30) with temperature dependency be unregularized (E_{λ} instead of $E_{\lambda,j}$) and just regularize the non-temperature dependent energy part. The question which of the two options is “better”, will be addressed later in detail.

In the energetical Pauli-Villars regularization scheme the regularized energies are defined [Nic09b, NB09] as

$$E_{\lambda,j} = \sqrt{E_{\lambda}^2 + j\Lambda^2}, \quad (3.32)$$

where Λ is the regulator-cutoff. In the case of 2SC and chirally broken phases three regulators in the thermodynamic potential eq. (3.30) are sufficient to render the integration finite ($r_{\text{PV}} = 3$). The coefficients c_j have to fulfill

$$\sum_i c_i = 0,$$

$$\sum_i c_i (M^2 + i\Lambda^2) = \sum_i c_i M_i^2 = 0$$

and

$$\sum_i c_i M_i^4 = 0.$$

Our particular choice for three regulators will be $c_0 = -c_3 = 1, c_1 = -c_2 = -3$.

If the thermodynamic potential is evaluated severe problems arise also in this regularization scheme. The self-consistent solution of the chiral condensate has an unwanted μ -dependency even below a critical value. Physically it is known, that for massive fermions the ground state of a quark system does not depend on the value of the chemical potential until a critical value μ_0 is reached. But since there is at least one quantity - the functional determinant of the Dirac operator - which depends on the value of the chemical potential, it is a puzzling question, why the system does not show any physical effect for varying chemical potential $\mu \leq \mu_0$ even if it should, because the observables of the system depend formally on the fermion determinant and as a consequence also the system depends on the chemical potential. This is known as the Silver Blaze property [Coh03]. Also for our case there should happen nothing below a critical value of the chemical potential, but as Fig. 3.1 suggests this regularization scheme produces results which contradict with this assumption. This is an undesired effect in the NJL model and is an artefact of the energetical Pauli-Villars like regularization. Algebraically these artefacts are caused by the following: For a system of quarks with homogeneous phases the eigenenergies of the Hamiltonian are given in energetical Pauli-Villars regularization by

$$\epsilon_{\pm,j} = \sqrt{\epsilon_{\pm}^2 + j\Lambda^2} = \sqrt{(\epsilon \pm \mu)^2 + j\Lambda^2} = \sqrt{\left(k^2 + M^2 \pm 2\sqrt{k^2 + M^2}\mu + \mu^2\right) + j\Lambda^2}$$

and

$$E_{\pm,j} = \sqrt{E_{\pm}^2 + j\Lambda^2} = \sqrt{\left(\sqrt{\epsilon_{\pm}^2 + |\Delta|^2}\right)^2 + j\Lambda^2} = \sqrt{k^2 + M^2 \pm 2\sqrt{k^2 + M^2}\mu + \mu^2 + |\Delta|^2 + j\Lambda^2}.$$

Inserting this in the thermodynamic potential eq. (3.30) it becomes finite, but through the nested square-root in the outer square-root

$$\sqrt{k^2 + M^2 \pm 2\sqrt{k^2 + M^2}\mu + \mu^2 + j\Lambda^2}$$

the minimum of the thermodynamic potential with respect to the dynamical mass M becomes rising with increasing μ , like shown in Fig. 3.1, where the increase of the mass M already starts at $\mu = 0$.

Since this undesired behavior occurs even in a system with only a scalar quark-antiquark interaction this regularization scheme will be discarded. Because of the attractivity of invariances in this procedure a similiar scheme should be used however, but it should not show unphysical artefacts.

3.3.3 Pauli-Villars regularization

In analogy to the energetical Pauli-Villars regularization a Pauli-Villars (PV) regularized thermodynamic potential is proposed in this thesis for homogeneous and inhomogeneous phases. This regularization scheme does not show the unwanted rising of the mass M with increasing chemical potential μ . Here the solution of the gap equation is fixed with respect to μ and the regularized energies of the thermodynamic potential eq. (3.30) in the non-temperature dependent part are given by

$$E_{\pm,j} := \sqrt{\left(\sqrt{k^2 + M^2 + j\Lambda^2} \pm \mu\right)^2 + |\Delta|^2} \quad (3.33)$$

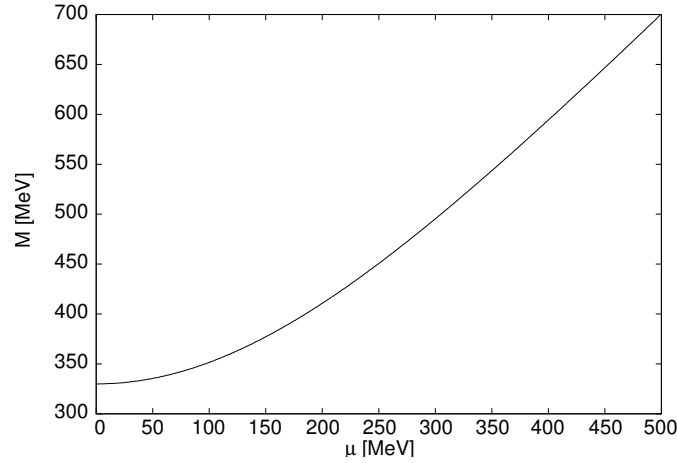


Figure 3.1.: Chemical potential dependency of the dynamical constituent mass M at $T = 0$ MeV. The parameters were chosen to obtain $M = 330$ MeV in vacuum and the rising of the constituent mass with increasing μ is an unwanted artefact below $\mu \leq \mu_c$.

and

$$\epsilon_{\pm,j} := \left(\sqrt{k^2 + M^2 + j\Lambda^2} \pm \mu \right), \quad (3.34)$$

which corresponds to the regularization of the divergent part by substituting

$$M^2 \rightarrow M_j^2 = M^2 + j\Lambda^2 \quad (3.35)$$

in the eigenenergies eqs. (3.25) and (3.26). This is also equal to replacing the energies by

$$\epsilon^2 = k^2 + M^2 \rightarrow \epsilon_j^2 = \epsilon^2 + j\Lambda^2. \quad (3.36)$$

In direct comparison the only difference between the energetical Pauli-Villars and Pauli-Villars regularization is the exact definition of the regulators. For the first scheme the overall free energies are replaced and for the latter only the mass is substituted, which is close to the original idea of Pauli and Villars.

Since there are no unexpected or unwanted artefacts in the regions of interest, the Pauli-Villars regularization scheme is also applied to inhomogeneous phases, where no momentum modes or other important quantities are (physically) restricted. Since for this reason this regularization scheme is best suited for our purposes of comparing chirally broken and color-superconducting phases it will be used throughout this thesis, if not otherwise stated. Even if a model does not include chirally broken (in)homogeneous phases or current masses we will still introduce mass regulators M_j in our calculations and afterwards set the mass M in the regulator to zero, which is necessary to establish a consistent treatment of our regularization scheme.

3.3.4 On the regularization of temperature-dependent diverging parts in the thermodynamic potential

If we want to check the validity of our regularization scheme also certain limits should be reproducible, like the Stefan Boltzmann law in the high temperature limit. As already briefly discussed the regularization of the temperature dependent part in eq. (3.30) is in general not necessary to yield finite results. Also

Table 3.1.: Overview over the different regularization schemes with their regulators and corresponding regularized thermodynamic potentials. The regularization of the temperature dependent part $\int d^3k \sum_{\lambda} (2T \log(1 + \exp(-E_{\lambda}/T)))$ is generally possible, but not necessary. As a this alters also the expression of the thermodynamic potential within one regularization scheme, we treat this as two separate cases of the same regularization mechanism. Here the prefactor $c \in \mathbb{R}$ was introduced for brevity, $\epsilon^2 = k^2 + m^2$ and E_{λ} denotes the eigenvalues of the Hamiltonian.

1. All diverging parts regularized

Regularization scheme	Regulators	Thermodynamic potential Ω_0
Energetical Pauli-Villars [3.3.2]	$E_{\lambda,j}^2 = E_{\lambda}^2 + j\Lambda^2$	$c \int d^3k \sum_{\lambda} \sum_j c_j \left(E_{\lambda,j} + 2T \log \left(1 + e^{-E_{\lambda,j}/T} \right) \right)$
Pauli-Villars [3.3.3]	$\epsilon_j^2 = \epsilon^2 + j\Lambda^2$	$c \int d^3k \sum_{\lambda} \sum_j c_j \left(E_{\lambda,j} + 2T \log \left(1 + e^{-E_{\lambda,j}/T} \right) \right)$

2. Only non-temperature dependent diverging parts regularized

Regularization scheme	Regulators	Thermodynamic potential Ω_0
Energetical Pauli-Villars [3.3.2]	$E_{\lambda,j}^2 = E_{\lambda}^2 + j\Lambda^2$	$c \int d^3k \sum_{\lambda} \left(\sum_j c_j E_{\lambda,j} + 2T \log \left(1 + e^{-E_{\lambda}/T} \right) \right)$
Pauli-Villars [3.3.3]	$\epsilon_j^2 = \epsilon^2 + j\Lambda^2$	$c \int d^3k \sum_{\lambda} \left(\sum_j c_j E_{\lambda,j} + 2T \log \left(1 + e^{-E_{\lambda}/T} \right) \right)$

Note: For the energetical Pauli-Villars regularization the regulators are identical to the regularized overall energies, but for the Pauli-Villars regularization scheme the energies are obtained by substituting $\epsilon^2 = k^2 + M^2$ in the unregularized eigenenergies with the regulator $\pm \epsilon_j$ which yields $E_{\lambda} \rightarrow E_{\lambda,j} = E_{\lambda}|_{\epsilon^2 \rightarrow \epsilon_j^2}$.

the values of the condensates do not differ significantly from each other, if the temperature-dependent part of the thermodynamic potential is regularized or not. The phase boundaries in the $\mu - T$ phase diagram also look qualitatively the same and especially for the 2SC phase are not distinguishable from the other possibility of a regularized or not regularized temperature part.

For high temperatures the thermodynamic potential eq. (3.30) with regularized temperature dependent part $T \cdot (\ln(1 + \exp(-E_{\lambda,j}/T)))$ does not converge to the value of the Stefan-Boltzmann limit. The value of this limit is given by calculating the pressure of a massless fermion $\nu = 2N_c N_f$ (+ antiparticles) degenerate gas, which corresponds to just evaluating the temperature dependent part of eq. (3.24)

$$\begin{aligned}
 p &= 12 \frac{4\pi T}{(2\pi)^3} \int_0^{\infty} dk k^2 \sum_{i=\pm} \left(\log \left(1 + \exp \left(-\frac{\epsilon_i}{T} \right) \right) \right) \\
 &= \frac{21}{90} \pi^2 T^4 + \mu^2 T^2 + \frac{\mu^4}{2\pi^2},
 \end{aligned} \tag{3.37}$$

where we used that for high temperatures $M = \Delta = 0$ holds and solved the occurring integral by partial integration analytically. If we divide in the next step by the fourth power, this ratio converges to the value

$$\lim_{T \rightarrow \infty} \frac{1}{T^4} \Omega(T, \mu = 0) \approx -2.303, \quad (3.38)$$

which is known as the Stefan-Boltzmann limit for high temperatures.

This limit is related to the regularization of the latter temperature-dependent part of the thermodynamic potential and the reproduction or non-reproduction of this value enables to decide if there is a physical difference between regularizing or not regularizing temperature dependent diverging terms. In Fig. 3.2 the thermodynamic potential $\Omega(T, \mu)$ over T^4 is plotted against the temperature. Because of the relation between the pressure and the chemical potential $p = -\Omega(T, \mu)$ the ratio $\Omega(T, \mu)/T^4$ is directly related to the above given limit, which we will evaluate for zero chemical potential. For regularizing all diverging terms in the thermodynamic potential this limit is not reproduced. If only the non-temperature dependent diverging parts of the thermodynamic potential Ω are regularized this limit is correctly fulfilled.

The correct reproduction of this limit is however less important for our analysis, because we mainly focus on low temperatures and therefore also the second part can be regularized. An overview of the different regularization methods and the possibilities for the regulators therein is presented in Tab. 3.1.

For the thesis the thermodynamic potential is given by

$$\Omega(T, \mu; M, \Delta) = -\frac{1}{4} \int \frac{d^3k}{(2\pi)^3} \sum_{\lambda} \left(\sum_{j=0}^{r_{PV}} c_j E_{\lambda,j} + 2T \ln(1 + \exp(-E_{\lambda}/T)) \right) + \frac{|M - m|^2}{4G} + \frac{|\Delta|^2}{4H}, \quad (3.39)$$

where the temperature-dependent part remains unregularized. In general one can use both possibilities for our case of low temperatures.

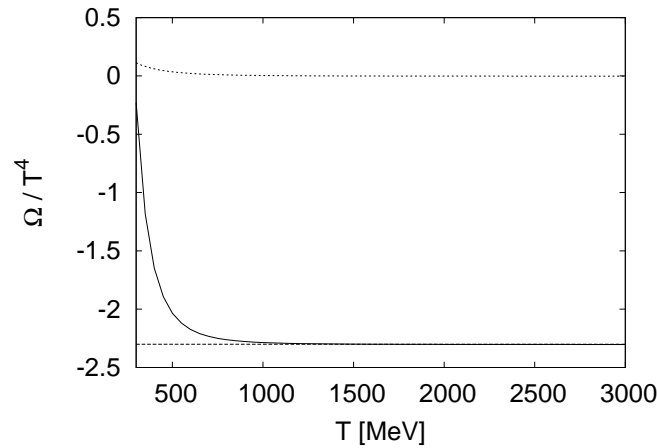


Figure 3.2.: The ratio of the grand potential $\Omega = -p$ and temperature to the fourth power T^4 against temperature T at $\mu = 0$ MeV. Only the regularization of non-temperature dependent diverging terms (solid) in the thermodynamic potential approaches the Stefan-Boltzmann limit (dashed), in contrast of regularizing all diverging terms (dotted).

3.3.5 Parameters

For the thermodynamical quantities in PV-regularization there are three unknown parameters in our NJL-model: The coupling constants G and H and the cutoff Λ . Experimentally there are only two known

Table 3.2.: Parameter set for our calculations in Pauli-Villars regularization.

Λ [MeV]	$G\Lambda^2$	H/G	M [MeV]
728.368	6.6	1/2	330

physical quantities, which can also be calculated in our model: The pion decay constant and the quark condensate density. Thus it is clear that our determination of the parameters suffers from an under-determination and only two parameters can be obtained independently, which are G and Λ . It also turns out that the value of the chiral condensate in the Pauli-Villars regularization scheme is smaller than “realistic” values suggest and this issue is bypassed by demanding a fixed value of the constituent quark mass in vacuum instead of the condensate density. Then we have to select how many regulators r_{PV} are used and insert the fixed mass M in the formula of the pion decay constant $f_\pi = 88 \text{ MeV}$ in the chiral limit

$$f_\pi^2 = -\frac{N_c M^2}{4\pi^2} \sum_{j=0}^{r_{\text{PV}}} c_j \log \frac{M^2 + j\Lambda^2}{M^2} \quad (3.40)$$

[Kle92] to obtain a value for the cutoff Λ . For given Λ and M this enables to determine the coupling constant G from the gap equation eq. (3.29) for $\mu \rightarrow 0$ in Pauli-Villars regularization

$$M = \frac{GN_f N_c M}{2\pi^2} \sum_{j=0}^{r_{\text{PV}}} (M^2 + j\Lambda^2) \log \left(\frac{M^2 + j\Lambda^2}{M^2} \right) \quad (3.41)$$

[Kle92] for $N_c = 3$, $N_f = 2$.

Our set of “realistic” parameters (Λ , G , H) is presented in Tab. 3.2 for three regulators and constituent quark mass $M = 330 \text{ MeV}$. The value of the diquark coupling constant H cannot be obtained from vacuum properties and the application of a Fierz transformation to the one-gluon exchange term gives $H/G = 3/4$. Since there is no real determination scheme for the coupling constant H also other values are valid, which changes the critical chemical potential, which is the value where the chiral condensate vanishes and the magnitude of the diquark condensate, as shown in Fig. 3.3 for some ratios of H/G . For the reproduction of “realistic”¹ diquark gaps we choose the ratio H/G to be 1/2, instead of 3/4.

¹ Values around $\Delta \approx 100 \text{ MeV}$.

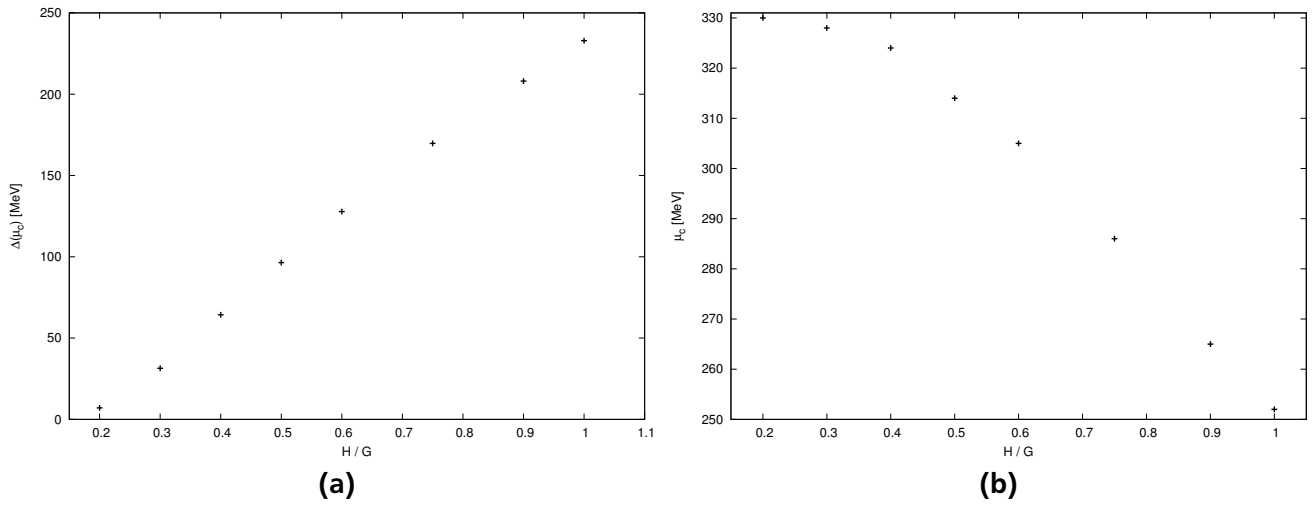


Figure 3.3.: (a) Diquark gap Δ at the critical chemical potential μ_c , where the chirally broken phase vanishes, for different values of the coupling constant H . (b) Critical chemical potential $\mu_c(H/G)$ for different couplings in the quark-quark channel.

4 Interplay of homogeneous and inhomogeneous phases

In the following chapter we study the interplay of homogeneous and inhomogeneous phases for quarks with two flavors. First, we calculate the phase boundaries of a homogeneous chirally broken and a 2SC phase at same chemical potentials $\mu_u = \mu_d$ and then analyse the effects of additionally including an inhomogeneous chirally broken phase.

Beside that we also consider up and down quarks with different chemical potential $\mu_u \neq \mu_d$ which allows for the appearance of inhomogeneous color-superconducting phases. To understand their appearance, another part of this chapter focuses on inhomogeneous 2SC phases and the effects of these condensates on the phase diagram.

For the whole analysis we will stay in the chiral limit $m = 0$. In general we minimize the thermodynamic potential $\Omega(T, \mu; \tilde{q})$ numerically with respect to the condensates \tilde{q} to obtain a self-consistent solution for the order parameters.

4.1 Homogeneous 2SC phase and homogeneous chirally broken phase

To begin our analysis we study the phase diagram of a system with chirally broken and 2SC phases described by the thermodynamic potential eq. (3.30) in Pauli-Villars regularization. At this stage we require the order parameters for the condensates to be constant in space, which is accomplished by neglecting any spatial dependency of the condensates eqn. (3.12) and (3.13).

For sufficiently low $\mu < \mu_c(T)$ the chiral condensate has a non-zero expectation value, which can be seen in Fig. 4.1, where the self-consistent solution of the mass in vacuum has the value predefined in the parameter fitting. This value remains finite and non-zero if the chemical potential is increased to non-zero values, but is still below the critical threshold μ_c . Above this value the chiral condensate has a vanishing expectation value indicating the restoration of chiral symmetry. It is a first-order phase transition from the chirally broken to the 2SC or restored phase below a tricritical point. Above this point the transition is second-order, because we are in the limit of massless up and down quarks. For large enough chemical potential and sufficiently low temperatures the condensation of two quarks is favored. Since the energetical preference of the 2SC phase happens at smaller chemical potential than for a system with only chiral symmetry breaking phases, the position of the phase boundary between the chirally broken and 2SC or restored phase is shifted to smaller values. For $T = 0$ MeV we find that the phase-transition of chiral restoration occurs at $\mu_c \approx 313$ MeV. Of course the exact position of the phase transition depends on the ratio of H/G , where G is still fixed by the choice of our parameter set.

The phase diagram is presented in Fig. 4.2. Below $T \approx 70$ MeV and above $\mu \approx 310$ MeV we find that the 2SC phase is dominating over the restored and chirally broken phase. It is enclosed by a second-order phase transition line to the restored phase and undergoes a first-order phase transition to the chirally broken phase. The known BCS-relation eq. (2.1) approximately holds for the 2SC phase, as it can be seen in Tab. 4.1.

4.2 Homogeneous 2SC phase and inhomogeneous chirally broken phase

Extending our results from the previous section we want to study the interplay of homogeneous 2SC phases and inhomogeneous chirally broken phases. Thus the thermodynamic potential is evaluated for

Table 4.1.: Critical temperatures T_c of the 2SC phase and the diquark gap at zero temperature $\Delta(T = 0)$ for different values of the chemical potential.

μ [MeV]	$\Delta(T = 0)$ [MeV]	T_c [MeV]	$T_c/\Delta(T = 0)$
313	95.99	55	0.57
356	114.06	64	0.56
400	128.00	71	0.55
450	137.94	75	0.54

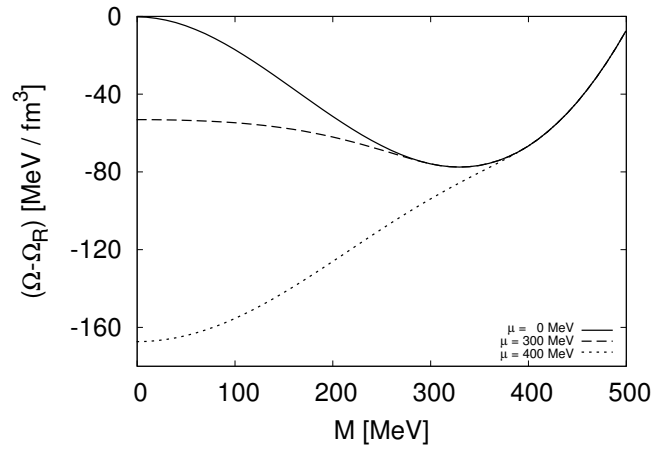


Figure 4.1.: Thermodynamic potential versus the dynamical constituent mass M for different chemical potentials.

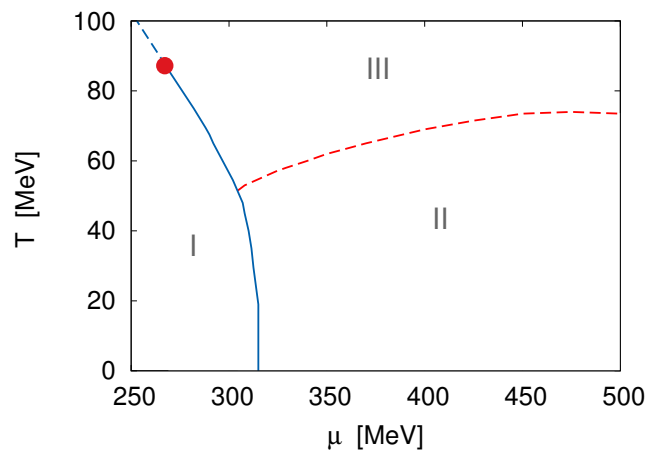


Figure 4.2.: The phase diagram for a system with a chirally broken phase (I), a 2SC phase (II) and the restored phase (III). First-order phase transitions are indicated by solid, second-order phase transitions by dashed lines and the tricritical point by the dot. Here the coupling constant H is fixed to $H/G = 0.5$.

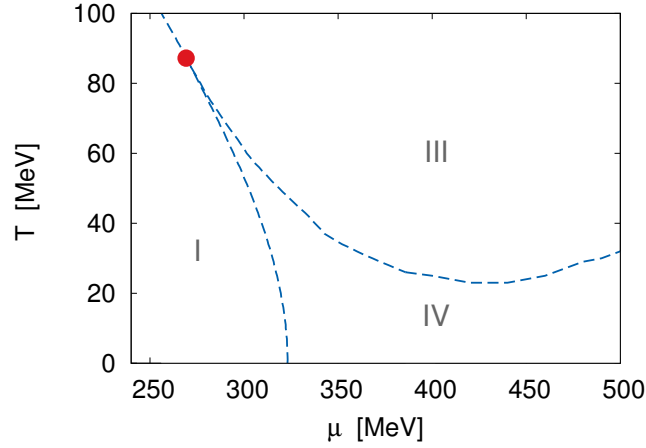


Figure 4.3.: The phase diagram of inhomogeneous chirally broken phases (IV), homogeneous chirally broken phases (I) and the restored phase (III). All boundaries of the inhomogeneous phases are second-order and the Lifshitz point is indicated by a dot [Carignano, 2011; private communication].

every point of the phase diagram for each phase. For the 2SC phase we still neglect any spatial dependency of the diquark condensates and use the previously obtained results. In contrast to our former calculations the chiral condensates are allowed to be spatially dependent. In this formalism it was found that an inhomogeneous phase appears in the region surrounding the chiral restoration phase transition for homogeneous condensates and completely covers the first-order phase transition, shown in Fig. 4.2. The inhomogeneous phase is enclosed by a second-order phase transition ending at a Lifshitz point, which in the simplest version of the model coincides with the critical point obtained for the homogeneous phases [Nic09a, Nic09b]. For the comparison of the different phases we assume that the phases do not mix with each other, i.e. $\phi(\vec{x}) = \langle \bar{\psi}\psi \rangle(\vec{x}) = 0$ if $s_{22} \neq 0$ and vice versa. The thermodynamic potential is regularized following the scheme proposed in sec. 3.3.3 to allow a consistent comparison between the (in)homogeneous chirally broken phase and the homogeneous 2SC phase. The comparison of the free energies allows us to determine which phase is dominant over other phases.

Using our standard parameter set we find (Fig. 4.4) that the homogeneous 2SC phase is favored over the inhomogeneous phase in a large region of the $\mu - T$ -phase diagram, although an inhomogeneous window persists in a region of the size $\Delta T = 16$ MeV and $\Delta\mu = 36$ MeV.

In our phase diagram two special points appear, where three phases (homogeneous 2SC, inhomogeneous and homogeneous chirally broken and restored phase, respectively) become degenerate.

The exact shape of the phase diagram is sensitive to the quark-quark coupling strength H . To illustrate this dependency we show several phase diagrams with different values of the quark-quark coupling constant H , while keeping G and Λ fixed.

In general these phase diagrams differ only at moderate temperatures and chemical potentials, where the difference of the thermodynamic potential of the different phases is small.

In Fig. 4.5 (a) the coupling strength in the quark-quark channel is increased, leading to a more favored 2SC phase and higher diquark gap. Inhomogeneous chirally broken phases survive only in a small region close to the Lifshitz point with a width of $\Delta\mu = 18$ MeV.

For lower quark-quark coupling on the other hand the inhomogeneous chirally broken phase extends to a region where the 2SC phase previously dominated for our standard choice $H/G = 0.5$. The resulting phase diagram Fig. 4.5 (b) shows that the intersection points of the different phases depart from their former position in μ and T direction and the first-order phase transition line between the inhomogeneous chirally broken phase to the homogeneous 2SC phase is extended.

If the coupling constant is decreased to even smaller values, like for $H/G = 0.3$, then the 2SC phase

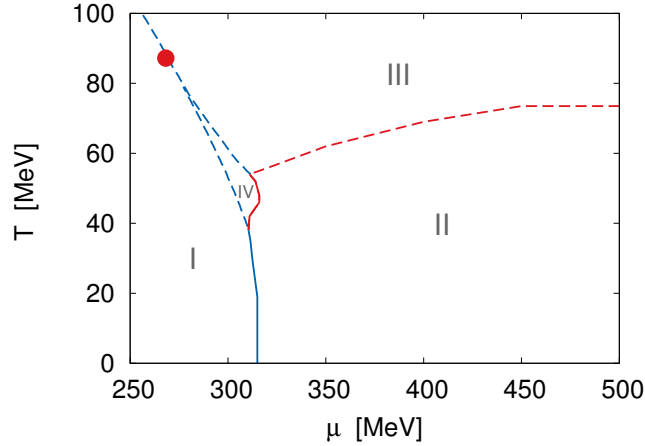


Figure 4.4.: The phase diagram for a homogeneous chirally broken phase (I), homogeneous 2SC phase (II), restored phase (III) and an inhomogeneous chirally broken phase (IV) in the chiral limit for $H/G = 0.5$. First-order phase-transitions are indicated by solid, second-order phase-transitions by dashed lines and the Lifschitz point by a dot.

does not intersect with the phase boundary of the homogeneous chirally broken phase any more. This is depicted in Fig. 4.5 (c), where the 2SC phase begins at $\mu = 345$ MeV. For the region around $\mu = 350$ MeV the 2SC phase competes with the inhomogeneous chirally broken phase and its boundary is shifted to higher chemical potential. This phase is enclosed by a first-order phase transition to the inhomogeneous chirally broken phase and extends up to a temperature $T = 25.5$ MeV.

For even weaker coupling $H/G = 0.2$ (Fig. 4.5 (d)) the phase diagram looks qualitatively the same but in contrast to the previous result the 2SC phase is always delimited by a first-order phase transition to the inhomogeneous chirally broken phase, which is favored at larger temperatures over the color-superconducting phase.

4.3 Inhomogeneous 2SC phases

Previously only homogeneous color-superconducting phases were taken into account for our analysis of strongly interacting quark matter. It is believed that color-superconducting phases with spatially dependent order parameter exist in the interior of neutron stars (for example, see [Red02]) and can play an important role for the exact structure of the phase diagram of quark matter.

For color superconductivity it was first suggested by Alford et al. [ABR01], that matter becomes inhomogeneous and condensed quarks form Cooper-pairs which are allowed to carry non-zero momentum $\vec{k}_{\text{tot}} \neq 0$.

Since the following derivation of the thermodynamic potential for inhomogeneous condensates is rather lengthy, we briefly outline our procedure: as a first step we derive the thermodynamic potential from the partition function and determine the effective Hamiltonian. Since it is still very difficult to determine the eigenenergies of the system from it we furthermore apply simplifications to reduce the size of the Hamiltonian.

Generalizing the formalism for homogeneous condensates in the framework above we mainly follow Nickel and Buballa [NB09] to allow for inhomogeneous condensates in color superconductivity. Additionally we keep a current mass m in the Lagrangian, which is needed for a consistent description of our regularization scheme. We introduce a flavor-dependent chemical potential $\mu_{u,d}$ for the up and down quarks

$$\mu_{u,d} = \bar{\mu} \pm \delta\mu, \quad (4.1)$$

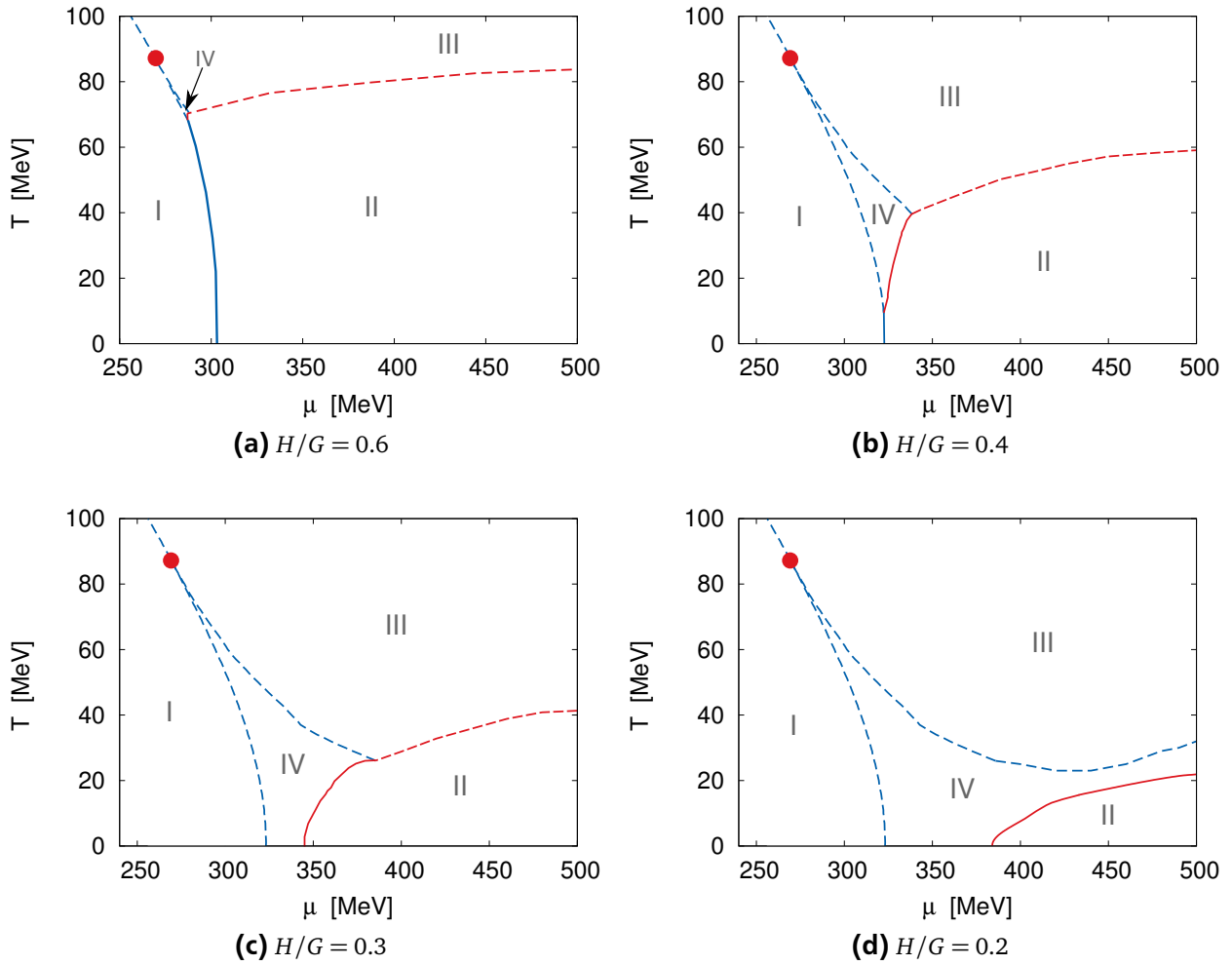


Figure 4.5.: The phase diagrams for a homogeneous 2SC phase (II), a homogeneous chiral phase (I), an inhomogeneous chirally broken phase (IV) and the restored phase (III) for different couplings H .

in our calculations for the two-flavor NJL Lagrangian. The quark-antiquark interaction $\mathcal{L}_{\bar{q}q}$ is neglected, because for now we are only interested in inhomogeneous 2SC phases. Explicitly this chemical potential difference of the two quark flavors is inserted in the Lagrangian eq. (3.2) via

$$\mathcal{L}_0 = \bar{\psi} \left(i\partial + (\bar{\mu} + \delta\mu \tau^3)\gamma^0 - m \right) \psi, \quad (4.2)$$

where τ^3 acts in flavor space.

We start with the linearization of the Lagrangian \mathcal{L}_{qq} , as presented before in eq. (3.14) for homogeneous 2SC and chirally broken phases. Instead of assuming a constant order parameter we still keep the spatial dependence in the condensate $s_{22} = s_{22}(\vec{x})$, which will be of major importance for inhomogeneous phases.

For an NJL model with three flavors more possible pairing patterns for inhomogeneous phases can occur, because there are more degrees of freedom for condensation than for the 2SC phase alone. Since we focussed on two-flavor color-superconductivity this topic is not investigated further, but the general formalism is presented for example in the work of Nickel and Buballa [NB09] or others.

For an inhomogeneous color-superconducting phase the expectation value $\langle \psi^T C \gamma_5 \tau_2 \lambda_2 \psi \rangle(\vec{x}) = -2H\Delta(\vec{x})$ for the 2SC condensate is still spatially varying and introducing bispinors in the Nambu-Gor'kov formalism leads to the Lagrangian

$$\begin{aligned} \mathcal{L} &= \bar{\Psi} \begin{pmatrix} i\partial + \hat{\mu} - m & \Delta(\vec{x})\tau_2\lambda_2\gamma_5 \\ -\Delta^*(\vec{x})\tau_2\lambda_2\gamma_5 & i\partial - \hat{\mu} - m \end{pmatrix} \Psi - \frac{1}{4H} |\Delta(\vec{x})|^2 \\ &\equiv \bar{\Psi} S^{-1} \Psi - \mathcal{V}, \end{aligned} \quad (4.3)$$

with $\hat{\mu} := (\bar{\mu} + \delta\mu \tau^3)\gamma^0$ and $\Psi, \bar{\Psi}$ denote Nambu-Gor'kov bispinors. Plugging the Lagrangian eq. (4.3) into eq. (3.21) and trying to evaluate the thermodynamic potential turns out to be very difficult due to an arbitrary spatial dependence of the Nambu-Gor'kov propagator S^{-1} .

We assume a static periodic structure for the energy gap $\Delta(\vec{x})$, which on the one hand is necessary to simplify the trace and perform the Matsubara sum and on the other hand allows to expand the entry Δ of the inverse propagator in a Fourier series with coefficients Δ_{q_k}

$$\Delta(x) = \sum_{q_k} \Delta_{q_k}(x) \exp(-iq_k x). \quad (4.4)$$

The momenta $q_k = (0, \vec{q}_k)^T$ form a reciprocal lattice, because of the Pontryagin duality between space and momentum, which, roughly speaking, tells how position space and momentum space are connected, and restricts the coefficients of the series according to

$$\vec{q}_k \cdot \vec{a}_i = 2\pi N_{k_i}, N_{k_i} \in \mathbb{Z} \quad (4.5)$$

where \vec{a}_i are the vectors spanning the unit cell of the crystal. These vectors give a measure of the periodicity

$$\Delta(\vec{x} + \vec{a}_i) = \Delta(\vec{x}) \quad (4.6)$$

of the diquark condensate.

Assuming periodic boundary conditions for the bispinors within the volume V and requiring that the unit cell is spanned by multiples $N \in \mathbb{N}$ of the vectors \vec{a}_i , allows to expand them in momentum space according to

$$\Psi(x) = \frac{1}{\sqrt{V}} \sum_{p_n} \Psi_{p_n} \exp(-ip_n x) \quad (4.7)$$

$$\bar{\Psi}(x) = \frac{1}{\sqrt{V}} \sum_{p_n} \bar{\Psi}_{p_n} \exp(ip_n x), \quad (4.8)$$

where the momentum $p_n = (i\omega_n, \vec{p}_n)^T$ has to satisfy the condition

$$\vec{p}_n \cdot \vec{a}_i = 2\pi \frac{N_{ni}}{N}, \quad N_{ni} \in \mathbb{Z}, \quad (4.9)$$

and ω_n denotes fermionic Matsubara frequencies. Thus the reciprocal lattice is N times more coarse than the mesh formed by the three-momenta.

The thermodynamic potential Ω is determined in the same way as for homogeneous phases. The only peculiarity here is the spatial dependence. For a better understanding this is sketched here: In terms of functional integration the partition function can be written as

$$\mathcal{Z} = \int \mathcal{D}\Psi \mathcal{D}\bar{\Psi} \exp S_E, \quad (4.10)$$

where S_E denotes the Euclidean action

$$S_E = \int_0^\beta d\tau \int d^3x \mathcal{L}(x^0 = -i\tau, \vec{x}) \quad (4.11)$$

in imaginary time formalism. Inserting the Lagrangian eq. (4.3) in the action (see App. A.2 for details)

$$\begin{aligned} S_E = \int_0^\beta d\tau \int d^3x & \left(\frac{1}{V} \sum_{p_m} \bar{\Psi}_{p_m} \exp(ip_m x) \times \right. \\ & \left(\begin{array}{cc} i\not{d} + \hat{\mu} - m & \sum_{q_k} \Delta_{q_k} \tau_2 \lambda_2 \exp(-iq_k x) \gamma_5 \\ -\sum_{q_k} (\Delta_{q_k} \tau_2 \lambda_2)^* \exp(iq_k x) \gamma_5 & i\not{d} - \hat{\mu} - m \end{array} \right) \times \\ & \left. \sum_{p_n} \Psi_{p_n} \exp(-ip_n x) - \frac{1}{4H} \sum_{q_k} |\Delta_{q_k}|^2 \right) \end{aligned} \quad (4.12)$$

can be used in the partition function to get an explicit expression for it, where eqs. (4.7), (4.8) and (4.4) are applied.

The thermodynamic potential is obtained by

$$\Omega(T, \mu) = -\frac{1}{V\beta} \ln \mathcal{Z}(T, \mu) \quad (4.13)$$

$$= -\frac{1}{2} \frac{1}{V\beta} \text{tr} \ln (\beta S^{-1}) + \sum_{q_k} \frac{|\Delta_{q_k}|^2}{4H}, \quad (4.14)$$

and is similar to the former result, but here the condensates are allowed to vary spatially. The Fourier-transformed inverse propagator has a non-trivial momentum dependency. The (p_m, p_n) -component of the inverse propagator S^{-1} is given by

$$S_{p_m, p_n}^{-1} = \left(\begin{array}{cc} (\not{p}_n + \hat{\mu} - m) \delta_{p_m, p_n} & \sum_{q_k} \hat{\Delta}_{q_k} \gamma_5 \delta_{q_k, p_m - p_n} \\ -\sum_{q_k} \hat{\Delta}_{q_k}^* \gamma_5 \delta_{q_k, p_n - p_m} & (\not{p}_n - \hat{\mu} - m) \delta_{p_m, p_n} \end{array} \right), \quad (4.15)$$

where we defined $\hat{\Delta}_{q_k} = \Delta_{q_k} \tau_2 \lambda_2$.

Physically speaking this describes that different momenta are coupled through the gap(s) in the off-diagonals, which results from the fact that diquarks are allowed to carry non-zero momentum and S^{-1} is in general not diagonal in momentum space.

Since we assumed a spatial periodicity of the condensates, the evaluation of the trace in the thermodynamic potential eq. (4.14) is simpler than for the general case.

By assuming static condensates the inverse propagator is diagonal in the energies, which translates in a diagonal structure for the Matsubara frequencies ω_n (see App. A.2). This allows to rewrite the inverse propagator as in eq. (3.22) and the effective Hamiltonian is given by

$$\mathcal{H}_{\vec{p}_m, \vec{p}_n} = \begin{pmatrix} \left(\gamma^0 \vec{p}_n - (\bar{\mu} + \delta\mu \tau^3) + m\gamma^0 \right) \delta_{\vec{p}_m, \vec{p}_n} & - \sum_{\vec{q}_k} \hat{\Delta}_{q_k} \gamma^0 \gamma_5 \delta_{\vec{q}_k, \vec{p}_m - \vec{p}_n} \\ \sum_{\vec{q}_k} \hat{\Delta}_{q_k}^* \gamma_0 \gamma_5 \delta_{\vec{q}_k, \vec{p}_n - \vec{p}_m} & \left(\gamma^0 \vec{p}_n + (\bar{\mu} + \delta\mu \tau^3) + m\gamma^0 \right) \delta_{\vec{p}_m, \vec{p}_n} \end{pmatrix} \quad (4.16)$$

for the (p_m, p_n) component, where $\vec{p} := \vec{\gamma} \vec{p}$ was introduced for notational brevity. Turning out the Matsubara sum yields the thermodynamic potential

$$\Omega(T, \mu) = -\frac{1}{4V} \sum_{\lambda} \left(E_{\lambda} + 2T \ln \left(1 + \exp \left(\frac{-E_{\lambda}}{T} \right) \right) \right) + \mathcal{V}, \quad (4.17)$$

which is formally the same as eq. (3.24) before taking the infinite volume limit. The energies E_{λ} are given by the eigenvalues of the Hamiltonian \mathcal{H} , which acts in Nambu-Gor'kov, Dirac, color, flavor and three-momentum space.

In principle this expression could be used to determine the thermodynamic potential, but the diagonalization is still complicated and numerically cost-expensive. This is our motivation to further simplify the structure of the Hamiltonian.

Through the Bloch theorem [Blo29] the symmetry of the effective Hamiltonian is connected to the symmetries of the static periodic condensates and thus the overall Hamiltonian eq. (4.16) can be decomposed into a simpler block diagonal form.

Physically the simplification correlates to the fact that only quarks in one block with the same vector of the Brillouin zone (B.Z.) can couple with each other and additionally the differences of their momenta have to be equal to q_n , which is an element of the reciprocal lattice (R.L.).

One block $\mathcal{H}(\vec{k}_n)$ looks formally the same like the Hamiltonian given in eq. (4.16), but the momenta can be written in the form

$$p_l = k_l + q_l, \quad (4.18)$$

for $l = m, n$, $k_l \in \text{B.Z.}$, $q_l \in \text{R.L.}$ and the Hamiltonian only needs to be diagonalized block-wise.

Inserting the decomposition of the total Hamiltonian in blocks in eq. (4.17)

$$\Omega(T, \mu) = -\frac{1}{4V} \sum_{\lambda} \left(E_{\lambda} + 2T \ln \left(1 + \exp \left(-\frac{E_{\lambda}}{T} \right) \right) \right) + \mathcal{V} \quad (4.19)$$

$$= -\frac{1}{4V} \sum_{\vec{k}_n \in \text{B.Z.}} \sum_{\lambda_k} \left(E_{\lambda_k}(\vec{k}_n) + 2T \ln \left(1 + \exp \left(-\frac{E_{\lambda_k}(\vec{k}_n)}{T} \right) \right) \right) + \mathcal{V} \quad (4.20)$$

yields in the infinite volume limit the thermodynamic potential

$$\Omega(T, \mu) = -\frac{1}{4} \int_{\text{B.Z.}} \frac{d^3k}{(2\pi)^3} \sum_{\lambda_k} \left(E_{\lambda_k}(\vec{k}) + 2T \ln \left(1 + \exp \left(-\frac{E_{\lambda_k}(\vec{k})}{T} \right) \right) \right) + \mathcal{V}, \quad (4.21)$$

where E_{λ_k} denote the eigenvalues of $\mathcal{H}(\vec{k}_n)$ (instead of \mathcal{H} as before), \mathcal{V} is the potential given in eq. (4.14) and the integration runs over the Brillouin zone.

4.3.1 Simplifications and approximations for inhomogeneous 2SC phases

The evaluation of the thermodynamic potential has effectively been reduced to the diagonalization of a block Hamiltonian, but is still very demanding, because on the one side the matrix representation of the Hamiltonian eq. (4.16) is still infinite in its size and also the diagonalization is very demanding. Hence we introduce additionally approximations and simplifications to reduce the complexity of the effective Hamiltonian. As a first step we remove the non-trivial structure resulting from the Dirac space in the off-diagonals for a block associated with vector \vec{k}_n :

$$(\mathcal{H}'(\vec{k}_n))_{\vec{p}_m, \vec{p}_n} = (U^\dagger \mathcal{H}(\vec{k}_n) U)_{\vec{p}_m, \vec{p}_n}, \quad (4.22)$$

where

$$U = \begin{pmatrix} \mathbb{1}_{4 \times 4} & 0 \\ 0 & \gamma^0 \gamma_5 \end{pmatrix}, \quad (4.23)$$

which yields

$$(\mathcal{H}'(\vec{k}_n))_{\vec{p}_m, \vec{p}_n} = \begin{pmatrix} (\gamma^0 \vec{p}_n - (\bar{\mu} + \delta\mu \tau^3) + m\gamma^0) \delta_{p_m, p_n} & \\ & \hat{\Delta}_{p_n - p_m} \\ & & -(\gamma^0 \vec{p}_n + (\bar{\mu} + \delta\mu \tau^3) + m\gamma^0) \delta_{p_m, p_n} \end{pmatrix}. \quad (4.24)$$

In general it is not possible to remove the whole Dirac structure for inhomogeneous phases simultaneously; it is only possible to trade off the vanishing of the non-trivial Dirac structure on the diagonal against the appearance in the off-diagonal or vice versa. Here we want to remove the structure on the diagonals, which in turn leads to a non-trivial Dirac structure in the off-diagonals. Only for the special case of homogeneous condensates no momentum modes are coupled via the gap and thus the whole structure can be absorbed in projectors on orthogonal subspaces and this allows to remove all of the Dirac structure from the effective Hamiltonian.

We however assume for the ongoing analysis of inhomogeneous 2SC phases that we can project out the Hamiltonian on orthogonal subspaces and for that define energy projectors

$$\Lambda_{\vec{p}}^\pm = \frac{1}{2} \left(1 \pm \gamma^0 \frac{\vec{p} + m}{\epsilon_{\vec{p}}} \right), \quad (4.25)$$

with

$$\epsilon_{\vec{p}} = \sqrt{\vec{p}^2 + m^2}.$$

Applying these projectors to the Hamiltonian eq. (4.24) the Dirac part on the diagonals becomes trivial

$$\gamma^0 (\vec{p} - \hat{\mu} \gamma^0 + m) = \left((-\hat{\mu} + \epsilon_{\vec{p}}) \Lambda_{\vec{p}}^+ + (-\hat{\mu} - \epsilon_{\vec{p}}) \Lambda_{\vec{p}}^- \right), \quad (4.26)$$

and the off-diagonals gain a non-trivial Dirac structure, which will not be taken into account for our approximation. This neglected part vanishes in the high density approximation, where the difference between the momenta p_i , $i = m, n$ is much smaller than the (averaged) chemical potential and only collinear scattering around the Fermi sphere takes place.

The remaining Hamiltonian is decomposed in a positive and negative energy part. Thus we are able to write

$$(\epsilon_n - \hat{\mu}) \begin{pmatrix} 1 & 0 \\ 0 & 0 \end{pmatrix} + (-\epsilon_n - \hat{\mu}) \begin{pmatrix} 0 & 0 \\ 0 & 1 \end{pmatrix} \equiv \mathcal{H}_{\mathcal{D}}^+ \oplus \mathcal{H}_{\mathcal{D}}^-, \quad (4.27)$$

where $\mathcal{H}_\mathcal{D}^\pm$ denotes the Hamiltonians with trivial Dirac structure associated to the orthogonal subspaces. Here we focused on the diagonals and also considered only the projection of one block. For the second block with non-trivial Dirac structure the projection is analogously performed and only the signs of $\hat{\mu}$ are interchanged. Then we are left with a structure given by

$$\left(\mathcal{H}''(\vec{k})\right)_{p_m, p_n} = \begin{pmatrix} (\epsilon_{\vec{p}_m} - \hat{\mu}) \delta_{\vec{p}_m, \vec{p}_n} & \hat{\Delta}_{p_m - p_n} \\ \hat{\Delta}_{p_n - p_m}^* & -(\epsilon_{\vec{p}_n} - \hat{\mu}) \delta_{\vec{p}_m, \vec{p}_n} \\ & -(\epsilon_{\vec{p}_m} + \hat{\mu}) \delta_{\vec{p}_m, \vec{p}_n} \\ & \hat{\Delta}_{p_n - p_m}^* & (\epsilon_{\vec{p}_m} + \hat{\mu}) \delta_{\vec{p}_m, \vec{p}_n} \end{pmatrix} \otimes \mathbb{1}_{2 \times 2}, \quad (4.28)$$

where \mathcal{H}'' is twice degenerate in its components, as indicated and the $\hat{\Delta}_{q_k}$'s still have a color-flavor structure. Particles and antiparticles do not mix and the Hamiltonian can be written as direct sum of the corresponding parts

$$\mathcal{H}'' = \mathcal{H}''_{\text{particles}} \oplus \mathcal{H}''_{\text{antiparticles}}, \quad (4.29)$$

where the vector \vec{k} in $\mathcal{H}''(\vec{k})$ will be suppressed for brevity in the following. The assumption that only red and green quarks pair allows to simplify the color-flavor structure of $\hat{\Delta}_{q_k}$, by decomposing the remaining structure of τ_2 and λ_2 into blocks.

For the simplified Hamiltonian eq. (4.28) the introduced difference between the up and down quark chemical potentials acts only in flavor space and therefore the Hamiltonian can be separated in a direct sum over the $\delta\mu$'s

$$\mathcal{H}'' = \mathcal{H}''_{\delta\mu=0} - \delta\mu \tau^3. \quad (4.30)$$

Inserting this Hamiltonian eq. (4.28) in the thermodynamic potential eq. (4.21) yields

$$\begin{aligned} \Omega(T, \mu) &= -\frac{1}{4} \int_{\text{B.Z.}} \frac{d^3k}{(2\pi)^3} \sum_{\lambda_k} \left(E_{\lambda_k}(\vec{k}) + 2T \ln \left(1 + \exp \left(-\frac{E_{\lambda_k}(\vec{k})}{T} \right) \right) \right) + \mathcal{V} \\ &= -\frac{1}{2} \int_{\text{B.Z.}} \frac{d^3k}{(2\pi)^3} \sum_{\lambda_k} \left(E''_{\lambda_k}(\vec{k}) + 2T \ln \left(1 + \exp \left(-\frac{E''_{\lambda_k}(\vec{k})}{T} \right) \right) \right) + \mathcal{V}, \end{aligned} \quad (4.31)$$

where E''_λ are the eigenvalues of the reduced Hamiltonian eq. (4.28).

The effective Hamiltonian eq. (4.28) can be written as a direct sum

$$\mathcal{H}'' = \bigoplus_{\substack{i = \pm\Delta \\ j = \pm\delta\mu \\ k = \pm\bar{\mu}}} \mathcal{H}''_{i,j,k}, \quad (4.32)$$

where we used eq. (4.30) and the fact that the dispersion relations of particles and antiparticles can be written independently from each other. The Hamiltonian is composed of different blocks characterized by the signs of the gaps, the average chemical potentials and the chemical potential mismatches. One direct summand is given by

$$\left(\mathcal{H}''_{i=\Delta, j=\delta\mu, k=\bar{\mu}}\right)_{\vec{p}_m, \vec{p}_n} = \begin{pmatrix} (\epsilon_{p_m} - \bar{\mu} - \delta\mu) \delta_{\vec{p}_m, \vec{p}_n} & \Delta_{p_m - p_n} \\ \Delta_{p_n - p_m}^* & -(\epsilon_{p_m} - \bar{\mu} + \delta\mu) \delta_{\vec{p}_m, \vec{p}_n} \end{pmatrix}, \quad (4.33)$$

where the gap-function $\Delta_{p_n - p_m}$ has to be specified for a certain phase and has a trivial color-flavor structure.

4.3.2 Regularization and parameters

Also for inhomogeneous color-superconducting phases the grand potential is divergent in the momentum integration and we follow the regularization scheme introduced in chap. 3.3.3 to render the diverging terms finite.

In the thermodynamic potential eq. (4.21) this can be done by applying the substitution eq. (3.35) to the energies $\pm\epsilon$ in the unregularized eigenvalues of the effective Hamiltonian. However this is more complicated than for the homogeneous case, since for inhomogeneous phases the eigenvalues are in general numerically calculated and the energy ϵ cannot be directly replaced according to $\epsilon^2 \rightarrow (\pm\epsilon_j)^2$. This substitution has to be done before calculating the eigenvalues. Here the sign of the $\pm\epsilon_j$ is of importance, since we have to regularize quark-quark resp. antiquark-antiquark pairs around their Fermi spheres.

The regularized thermodynamic potential is given as

$$\Omega(T, \mu) = - \int_{\text{B.Z.}} \frac{d^3k}{(2\pi)^3} \sum_{\lambda} \left(\sum_j c_j E_{\lambda,j}(\vec{k}) + 2T \ln \left(1 + \exp \left(-\frac{E_{\lambda}(\vec{k})}{T} \right) \right) \right) + \mathcal{V} \quad (4.34)$$

and E_{λ} are the eigenvalues of \mathcal{H}_{ijk}'' defined in eq. (4.33). This will be the starting point for our numerical evaluation.

The model parameters are given in Tab. 3.2. For the ongoing discussion it is convenient to express quantities in terms of Δ_{BCS} , where Δ_{BCS} is the diquark gap at $\delta\mu = 0$. This value parametrizes the coupling strength H at fixed $\bar{\mu}$. As before also for inhomogeneous condensates the coupling strength is not fixed a priori and can be varied. Here only our standard choice $H/G = 0.5$ is considered.

4.3.3 BCS phase

Turning to the well-known result by Bardeen et al. [BCS57], we analyse the occurrence of homogeneous Cooper-pairs in our theory. For that we assume a constant, homogeneous gap-function and allow a mismatch in the chemical potentials in our two-flavor model. The effective Hamiltonian for the homogeneous BCS-solution is given by

$$(\mathcal{H}_{\text{eff}})_{\vec{p}_m, \vec{p}_n} = \begin{pmatrix} (\epsilon_{\vec{p}_m} \pm (\bar{\mu} + \delta\mu \tau^3)) \delta_{\vec{p}_m, \vec{p}_n} & \Delta_{p_m - p_n} \\ \Delta_{p_n - p_m}^* & -(\epsilon_{\vec{p}_m} \pm (\bar{\mu} + \delta\mu \tau^3)) \delta_{\vec{p}_m, \vec{p}_n} \end{pmatrix}, \quad (4.35)$$

where

$$\Delta_{q_k} = \Delta \delta_{q_k, 0} \quad (4.36)$$

is the Fourier-transformed BCS gap-function and appears in the off-diagonals of the Hamiltonian. One direct summand of eq. (4.32) reads for this case

$$\left(\mathcal{H}_{\Delta, \bar{\mu}, \delta\mu}'' \right)_{\vec{p}_m, \vec{p}_n} = \begin{pmatrix} (\epsilon_{\vec{p}_m} - \bar{\mu} - \delta\mu) \delta_{\vec{p}_m, \vec{p}_n} & \Delta \delta_{p_m, p_n} \\ \Delta^* \delta_{p_m, p_n} & -(\epsilon_{\vec{p}_m} - \bar{\mu} + \delta\mu) \delta_{\vec{p}_m, \vec{p}_n} \end{pmatrix} \quad (4.37)$$

and the Hamiltonian eq. (4.35) has a block-diagonal shape, which allows to calculate the eigenvalues of eq. (4.35) by only diagonalizing the direct summands. All introduced simplifications from above are exact for this special case of homogeneous condensates and could also be obtained by evaluating eq. (4.24) directly.

Every block of the decomposed Hamiltonian has eigenvalues of the form

$$E_{\lambda} = \sqrt{(p \pm \bar{\mu})^2 + |\Delta|^2} \pm \delta\mu = \sqrt{\Delta^2 + p^2 \pm 2p\bar{\mu} + \bar{\mu}^2} \pm \delta\mu,$$

for momentum p .

If antiparticles are neglected the Hamiltonian can be further simplified to

$$\mathcal{H}'' = \mathcal{H}''_{\Delta, \delta\mu} \oplus \mathcal{H}''_{-\Delta, \delta\mu} \oplus \mathcal{H}''_{\Delta, -\delta\mu} \oplus \mathcal{H}''_{-\Delta, -\delta\mu}, \quad (4.38)$$

which halves the dimension of the problem.

This approximation would have only minor effects on the magnitude of the gap, because antiparticles do not contribute significantly for high μ .

The energetical Pauli-Villars regularization scheme leads to a $\delta\mu$ -dependency of the diquark gap, even for a fixed chemical potential $\bar{\mu}$. In contrast our chosen regularization scheme does not show these artefacts in the region of interest.

The gap is constant with respect to an increasing chemical potential mismatch at zero temperature below a critical value because of the cancelation of the two terms $+\delta\mu$ and $-\delta\mu$ in the sum over the (regularized) eigenenergies, like in the unregularized case for zero temperature

$$\Omega_{\text{unreg.}}(T=0, \bar{\mu}, \delta\mu) = -4 \int \frac{d^3p}{(2\pi)^3} \sqrt{(p - \bar{\mu})^2 + |\Delta|^2} + \frac{|\Delta|^2}{4H}, \quad (4.39)$$

where the $\delta\mu$ -dependency also drops out.

At an upper limit $\delta\mu_c$ the occurrence of BCS pairing is not favored any more over the restored phase. The minimum of the thermodynamic potential with respect to Δ remains constant if $\delta\mu$ is changed, whereas the thermodynamic potential for the unpaired quarks ($\Delta = 0$) alters with $\delta\mu$. This leads to a relative difference in the free energies of paired and unpaired quarks, which causes that at $\delta\mu_c$ the unpaired phase is energetically favored for the paired solution. This mechanism is analogous to the one for chirally broken phases with mass M and μ in Fig. 4.1, instead of Δ and $\delta\mu$.

In the weak coupling limit this critical chemical potential difference is $\delta\mu_c = 1/\sqrt{2} \Delta_{\text{BCS}}$ and was found by Chandrasekhar [Cha62] and Clogston [Clo62].

The *Fulde-Ferrell* (FF) phase or other inhomogeneous color-superconducting phases can tolerate higher chemical potential differences $\delta\mu$ and are then favored over the BCS phase.

For non-zero temperature there is a dependence on $\delta\mu$ for the thermodynamic potential through the eigenvalues of the effective Hamiltonian eq. (4.35) in the temperature dependent part.

In Fig. 4.6 the $\delta\mu - T$ phase diagram for the BCS phase is shown: Along the $\delta\mu$ axis the transition from the BCS to the restored phase is first-order. For small temperatures $T < 0.28\Delta_{\text{BCS}}$ the order remains unchanged. Above this point the BCS phase is connected to the restored phase by a second-order phase transition.

If there is no mismatch between the chemical potential of up and down quarks the BCS relation for the critical temperature is fulfilled, but otherwise the ratio T_c/Δ_{BCS} goes steadily down with increasing mismatch and becomes zero at $\delta\mu_c$.

For different chemical potentials $\bar{\mu}$ the $\delta\mu - T$ phase diagram looks qualitatively the same, but since Δ_{BCS} is $\bar{\mu}$ -dependent only the ratios $\delta\mu/\Delta_{\text{BCS}}$ are approximately equal.

In Fig. 4.7 the resulting phase diagrams for differing chemical potentials $\mu_u \neq \mu_d$ for a BCS phase and a homogeneous chiral phase are shown in the $\mu - T$ -plane. The chiral phase was just added for a better comparison to the previous phase diagrams and also exhibits stressed quark-antiquark pairing due to the chemical potential mismatch.

For small chemical potential mismatch the phase diagram looks like the one for $\delta\mu = 0$, but for larger chemical potential difference the BCS and chiral phase are present in smaller regions of the phase diagram. The BCS phase has lower critical temperatures than for the $\delta\mu = 0$ case, but is still connected to the chiral phase for $\delta\mu = 20 \text{ MeV}$ and $\delta\mu = 40 \text{ MeV}$, as shown in Figs. 4.7 (a) and (b). For small temperatures the phase transition line between the chiral and BCS phase starts at lower chemical potential than for $\delta\mu = 0$, then increases to larger $\bar{\mu}$ and for intermediate to large temperatures goes back to smaller

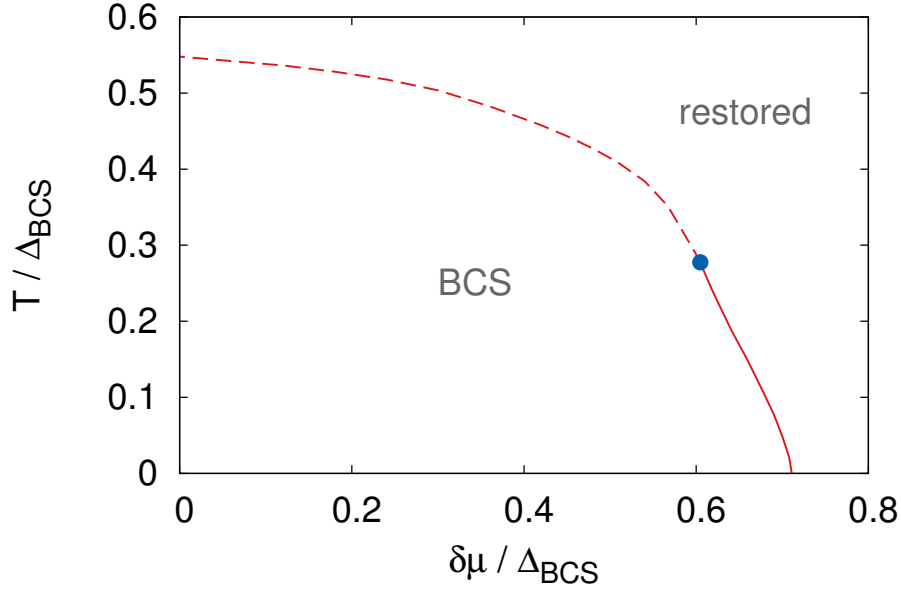


Figure 4.6.: The phase diagram for the BCS solution in the $\delta\mu - T$ -plane at $\bar{\mu} = 400$ MeV. The phase transition from the BCS to restored phase is of second-order (dashed) from $\delta\mu = 0$ until $\delta\mu \approx 0.61\Delta_{\text{BCS}}$ (blue dot) and then becomes first-order (solid).

values of the chemical potential. The shifting to smaller chemical potentials for low temperatures is only visible for $\delta\mu = 20$ MeV in the figure, although this effect happens on smaller scales for $\delta\mu = 40$ MeV (Fig. 4.7 (b)).

For larger mismatches the BCS and chiral phase have no common boundary and the BCS to restored phase transition is first-order. Above a critical chemical potential $\bar{\mu}$, where the ratio of $\delta\mu/\Delta_{\text{BCS}}$ drops below 0.61 the BCS phase is connected to the restored phase by a second-order phase transition, as shown for $\delta\mu = 76$ MeV in Fig. 4.7 (c). If the mismatch is further enlarged ($\delta\mu = 80$ MeV for Fig. 4.7 (d)) the phase is favored in smaller regions and the second-order phase transition begins at larger chemical potential $\bar{\mu}$.

In general for sufficiently large $\delta\mu \geq 0.71\Delta_{\text{BCS}}$ the BCS phase is energetically disfavored over the restored phase everywhere.

4.3.4 Fulde-Ferrell phase

In a homogeneous phase the gain in condensation energy and the energy cost for the modification of the Fermi spheres compete with each other. At some point the pairing can be disfavored over the condensation in inhomogeneous phases, where the Cooper-pairs are allowed to carry non-zero momentum. One of the simplest attempts to create inhomogeneous superconducting condensates was proposed by Fulde and Ferrell [FF64], where a gap function with a single plane-wave spatial modulation

$$\Delta(x) = \Delta \exp(2i\vec{q}\vec{x}), \quad (4.40)$$

was assumed, where \vec{q} denotes the wave-vector. In our framework the diquark condensate is allowed to have this spatial plane-wave modulation and in contrast to the previously considered gap-function it has complex values.

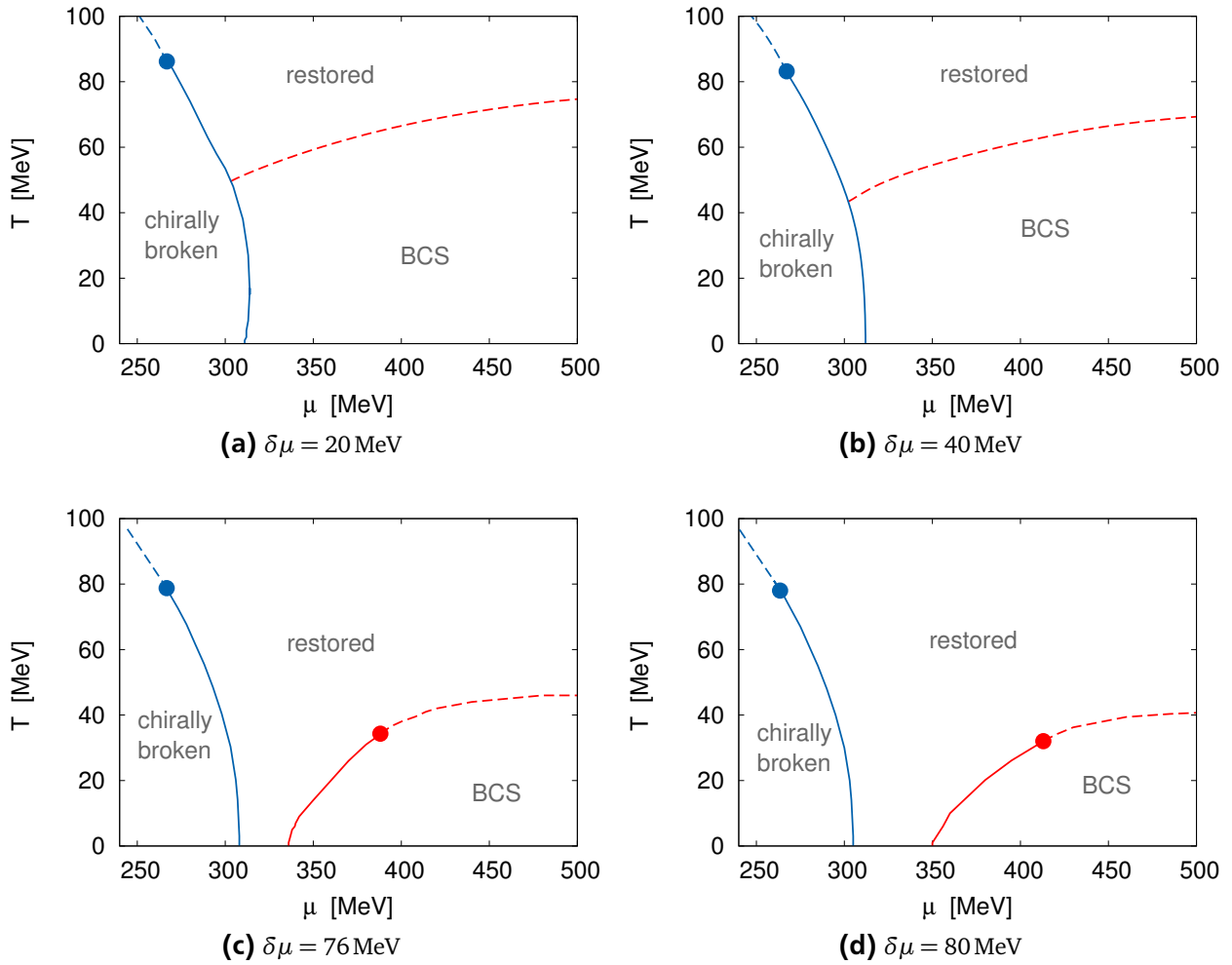


Figure 4.7.: Phase diagrams of a BCS and homogeneous chiral phase in the $\mu - T$ -plane for two flavors with differing chemical potential at fixed $\delta\mu$'s. Here the averaged chemical potential of up and down quarks is denoted by $\mu \equiv \bar{\mu}$.

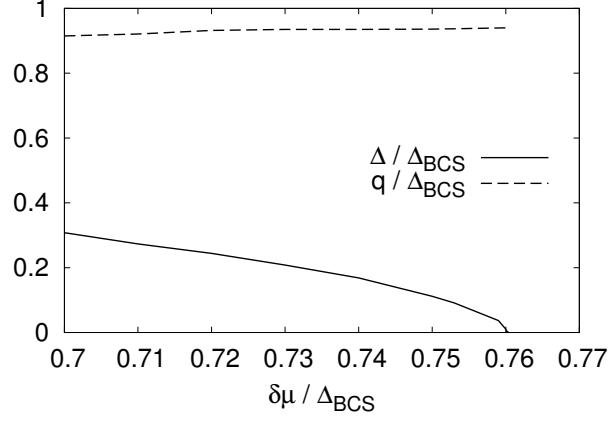


Figure 4.8.: Preferred value of the wave number $|\vec{q}|$ (dashed) and the corresponding amplitude of the Fulde-Ferrell gap Δ (solid) at $T = 0$ and $\bar{\mu} = 400$ MeV.

The Brillouin zone of the resulting crystal structure is infinite in the directions perpendicular to \vec{q} and finite with length $2|\vec{q}|$ in \vec{q} -direction. In the effective Hamiltonian

$$\left(\mathcal{H}_{\Delta, \bar{\mu}, \delta\mu}'' \right)_{\vec{p}_m, \vec{p}_n} = \begin{pmatrix} (\epsilon_{\vec{p}_m} - \bar{\mu} - \delta\mu) \delta_{\vec{p}_m, \vec{p}_n} & \Delta \delta_{\vec{p}_m - \vec{p}_n, 2\vec{q}} \\ \Delta^* \delta_{\vec{p}_n - \vec{p}_m, 2\vec{q}} & -(\epsilon_{\vec{p}_m} - \bar{\mu} + \delta\mu) \delta_{\vec{p}_m, \vec{p}_n} \end{pmatrix} \quad (4.41)$$

different momenta are coupled, where the Fourier-transformed Fulde-Ferrell gap

$$\Delta_{qk} = \Delta \delta_{\vec{q}_k, 2\vec{q}} \quad (4.42)$$

determines which momenta interact.

Normally the determination of an analytical expression for the eigenvalues is not possible within this general structure of the Hamiltonian, since there is no obvious finite block-diagonal form.

However it is still possible to identify in the Hamiltonian eq. (4.41) finite “shifted” blocks, where two momenta are coupled, which read

$$\begin{pmatrix} (\epsilon_+ - \hat{\mu}) & \Delta \\ \Delta^* & -(\epsilon_- - \hat{\mu}) \end{pmatrix}, \quad (4.43)$$

where $\epsilon_{\pm} = \sqrt{|\vec{k} \pm \vec{q}|^2 + m^2}$. The eigenvalues for the particles are given by

$$|E_{\pm}(\vec{k})| = \left| \frac{\epsilon_+ - \epsilon_-}{2} \pm \sqrt{\left(\frac{\epsilon_+ + \epsilon_-}{2} - \hat{\mu} \right)^2 + |\Delta|^2 - \delta\mu} \right|, \quad (4.44)$$

and analogously for the antiparticles. These eigenvalues simplify to the eigenvalues of the BCS case for $q = 0$. The block structure allows to rewrite the integration over the Brillouin zone to an integration over the whole space as

$$\int_{\mathbb{R}^2} d\vec{k}_{xy} \int_0^{2q} dk_z \sum_{\lambda_k} E_{\lambda_k} = \int_{\mathbb{R}^2} d\vec{k}_{xy} \int_0^{2q} dk_z \sum_i \sum_{\lambda_{k,i}} E_{\lambda_{k,i}} = \int_{\mathbb{R}^2} d\vec{k}_{xy} \int_{-\infty}^{\infty} dk_z \sum_{\lambda_{k,i}} E_{\lambda_{k,i}} = \int_{\mathbb{R}^3} d\vec{k} \sum_{\lambda_{k,i}=\pm} E_{\lambda_{k,i}}, \quad (4.45)$$

where $E_{\lambda_{k,i}}$ are the eigenvalues of the i -th block, which is given by eq. (4.43). In the thermodynamic potential only the eigenvalues per block have to be determined for its evaluation and with this identification

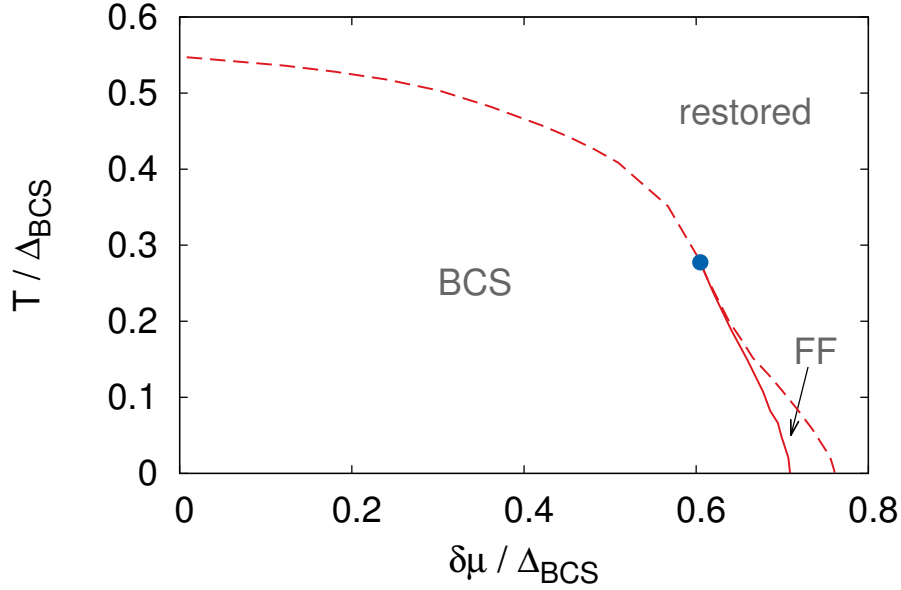


Figure 4.9.: Phase diagram for the BCS and Fulde-Ferrell phase. Here the line type indicates the order of the phase transition: first order (solid) and second-order(dashed) at $\bar{\mu} = 400$ MeV.

it is possible to circumvent the numerical evaluation of the eigenvalues of the Hamiltonian eq. (4.41), which is more time-consuming.

In general the thermodynamic potential for the Fulde-Ferrell (FF) phase depends on two values: the energy gap Δ and the wave vector q , which are shown in Fig. 4.8. The phase space of the Fulde-Ferrell phase is limited and thus the diquark condensate has a smaller value than for the BCS case, as confirmed by our numerical calculations. The wave number $|\vec{q}|$ is weakly rising throughout the window, where the Fulde-Ferrell phase is favored and is of the order of $0.9 \Delta_{\text{BCS}}$, whereas the diquark gap is smaller than for the BCS phase and goes down to zero for a critical chemical potential mismatch $\delta\mu_2$. The highest magnitude of the gap is about $\approx 0.35 \Delta_{\text{BCS}}$.

In the $\delta\mu$ - T phase diagram Fig. 4.9 the Fulde-Ferrell phase only appears for $\delta\mu \geq \delta\mu_1 = 0.709 \Delta_{\text{BCS}}$ and $\delta\mu \leq \delta\mu_2 = 0.76 \Delta_{\text{BCS}}$ at $T = 0$. For non-zero temperatures this $\delta\mu$ window decreases until the FF condensate is disfavored over the BCS or restored phase. The phase transition line between the restored and FF phase is of second-order, while the phase transition to the BCS phase is first-order.

The exact values for the critical chemical potential mismatch is known only for the weak-coupling limit to be $\delta\mu_1 = 1/\sqrt{2} \Delta_{\text{BCS}}$ and $\delta\mu_2 = 0.7602 \Delta_{\text{BCS}}$. The deviations between our result and the known values for weak-coupling should approach zero for $\Delta_{\text{BCS}} \rightarrow 0$, but this was not checked.

In the $\mu - T$ plane the Fulde-Ferrell phase is only present for large chemical potential differences $\delta\mu$. For $\delta\mu = 20$ MeV and $\delta\mu = 40$ MeV we find that only the BCS phase and the chiral phase appear in the phase diagram. For $\delta\mu = 80$ MeV there exists a region close to the $\bar{\mu}$ -axis where the Fulde-Ferrell phase is favored. Around the tricritical point the phase transition lines of the BCS and FF phase are nearly identical and for values $\bar{\mu} \geq 375$ MeV in Fig. 4.10 we cannot numerically distinguish between the FF and BCS phase, because their relative difference in the thermodynamic potential is too small. The thermodynamic potential of the Fulde-Ferrell phase is shown in Fig. 4.12 below for $T = 0$, where also the free energy of the Fulde-Ferrell phase is close to the one of the restored phase.

For $\delta\mu = 76$ MeV the FF phase is favored in a region around the BCS phase-transition and has a maximal width of $\Delta\mu = 18$ MeV.

In principle there should also be a $\delta\mu$, where the Fulde-Ferrell phase reaches to the phase boundary of

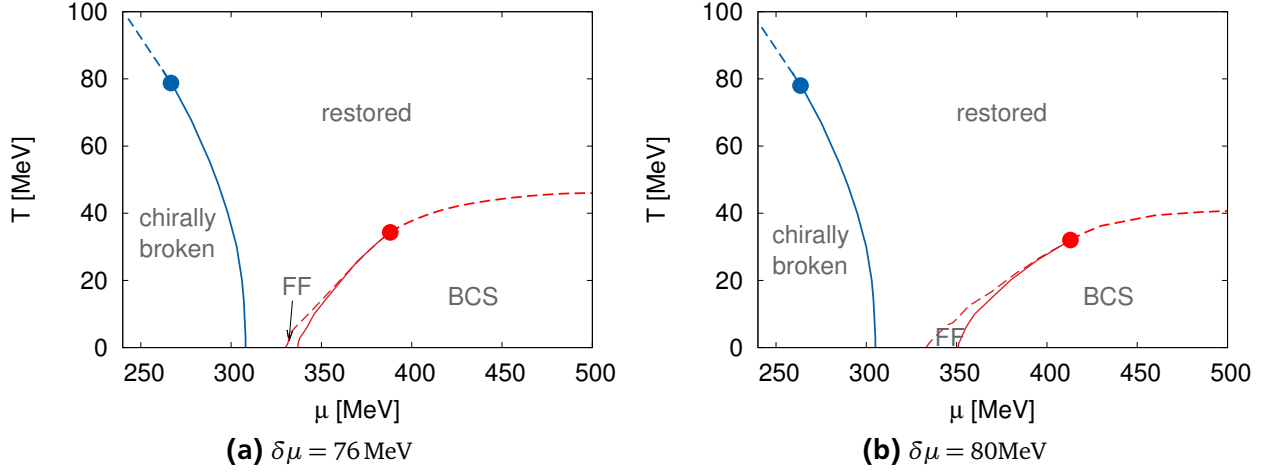


Figure 4.10.: The phase diagram of a BCS, chiral, Fulde-Ferrell and restored phase for different $\delta\mu$'s.

the chirally broken phase, but this has not been checked in detail. Our existing results indicate that this value should be around $\delta\mu \approx 65$ MeV.

4.3.5 General inhomogeneous phases in one dimension

In Ref. [NB09] it was shown that at zero temperature in the energetical Pauli-Villars regularization scheme gap functions with a general periodic structure in one dimension are favored over homogeneous phases for a $\delta\mu$ -window in two-flavor color superconductivity. For regions close to the critical value $\delta\mu_c$ of the BCS phase the authors observed the formation of a soliton lattice, which extends the onset of the window for inhomogeneous phases to lower $\delta\mu$ values, while the upper end remains close to the one of the Fulde-Ferrell phase. In our regularization scheme we also want to study the appearance of general inhomogeneous 2SC phases with an order parameter that varies in one dimension. Our previous results for color-superconducting phases were limited by the number of allowed harmonics. Here we consider a general periodic gap function

$$\Delta(\vec{x}) = \sum_k \Delta_{\vec{q},k} \exp(i\vec{q}_k \vec{x}) = \sum_k \Delta_{\vec{q},k} \exp(2ik\vec{q}\vec{x}). \quad (4.46)$$

The Brillouin zone is infinite in the directions perpendicular to \vec{q} and finite in the direction of \vec{q} , where this vector points without loss of generality in z -direction. Furthermore only real gap functions are considered, which means that $\Delta_{\vec{q},k} = \Delta_{\vec{q},-k}^*$ holds. One period corresponds to $z = \pi/q$. Inserting eq. (4.46) in the effective Hamiltonian eq. (4.33) yields

$$\left(\mathcal{H}_{\Delta, \delta\mu, \bar{\mu}}'' \right)_{\vec{p}_m, \vec{p}_n} = \begin{pmatrix} (\epsilon_{\vec{p}_m} - \bar{\mu} - \delta\mu) \delta_{\vec{p}_m, \vec{p}_n} & \sum_k \Delta_{2\vec{k}q} \delta_{p_m - p_n, 2kq} \\ \sum_k \Delta_{2\vec{k}q}^* \delta_{p_n - p_m, 2kq} & -(\epsilon_{\vec{p}_m} - \bar{\mu} + \delta\mu) \delta_{\vec{p}_m, \vec{p}_n} \end{pmatrix}, \quad (4.47)$$

where $\Delta_{\vec{q},k} \equiv \Delta_{2k\vec{q}}$, which is again an infinite matrix in momentum space and the sum over k in the off-diagonals couples multiple momenta.

For this Hamiltonian one does not find a transformation to a block-diagonal form with finite block-size and the eigenenergies have to be determined numerically.

Here our regularization scheme is applied, but has to be adapted for the numerical approach: First we

diagonalize the Hamiltonian, where Pauli-Villars regulators were already inserted. Then we sum over the eigenvalues to obtain a finite integral. The regularized thermodynamic potential is given by

$$\Omega(T, \mu) = -2 \int_{\text{B.Z.}} \frac{d^3k}{(2\pi)^3} \sum_j c_j \left(\sum_{\lambda} E_{\lambda,j}(\vec{k}) + \sum_{\lambda} 2T \ln \left(1 + \exp \left(-\frac{E_{\lambda,j}(\vec{k})}{T} \right) \right) \right) + \frac{1}{4H} \sum_{q_k} |\Delta_{q_k}|^2 \quad (4.48)$$

and $E_{\lambda,j}$ denotes the eigenvalues of the “regularized Hamiltonians”. Here we regularize all parts, not only the non-temperature dependent terms, although to be consistent with the former results only this part should be regularized. However for the homogeneous case it was checked, that the difference between the two schemes is so small, that a quantitative change in the $\delta\mu - T$ phase diagram is not visible. Only when going to very high temperatures the regularized resp. non-regularized temperature-dependent part of the thermodynamic potential differ in a direct comparison significantly.

Since the Hamiltonian is still infinite in its size the maximal allowed momenta must be restricted additionally. This is done by requiring

$$\left| \vec{k} \pm n_{\text{max}}(\vec{k}) \vec{q} \right| \leq \Lambda_M, \quad (4.49)$$

where the cutoff Λ_M makes the numerical evaluation tractable and $n_{\text{max}}(\vec{k})$ is the number of maximal allowed momenta in the Hamiltonian. In contrast to the Fulde-Ferrell phase, where only two momenta can interact via the gap, this is for a generic one-dimensional modulation more crucial, since all momenta can be coupled. The value of this upper boundary has to be chosen, so that the (physical) results do not alter.

The matrix size is given by

$$m_{\text{tot}} = 2 \cdot (2n_{\text{max}} + 1) \quad (4.50)$$

and the regularized Hamiltonian has to be numerically evaluated r_{PV} times, which slows down the calculations.

The condensate Δ and the wave vector q are obtained by minimizing the thermodynamic potential with respect to the Fourier components at fixed q and then when the solution is found, with respect to the energetically preferred value of q . For small $\delta\mu$ at the lower end of the $\delta\mu$ -window the wave vector approaches zero and the numerical analysis gets involved, since the period goes to infinity.

Since the numerical evaluation of generic inhomogeneous color-superconducting phases at several values of $\bar{\mu}$ would further increase the time needed for our calculations, we consider first a fixed average chemical potential $\bar{\mu} = 400 \text{ MeV}$.

The gap function $\Delta(z)$ looks for large q at fixed $\delta\mu$ like a sinusoidal modulation and for smaller q the formation of soliton lattice was found by Nickel and Buballa [NB09], where the gap remains nearly constant for a half-period and then changes its sign in a small interval of z .

In Fig. 4.11 the wave number q and the magnitude Δ at the energetically preferred value of q are plotted against $\delta\mu$. For small chemical potential mismatches the magnitude of the diquark gap remains constant up to $\delta\mu_1$, which we found to be below $\delta\mu_1 \leq 0.7\Delta_{\text{BCS}}$ but were not able to determine the exact value. At this lower bound the magnitude begins to decrease and at the same time the wave number q has non-zero values and increases to about $0.8\Delta_{\text{BCS}}$ for higher chemical potential differences. At $\delta\mu_2$ the generic inhomogeneous color-superconducting phase is disfavored over the restored phase and in our numerical calculations this happens between $0.76\Delta_{\text{BCS}}$ and $0.78\Delta_{\text{BCS}}$. In a direct comparison with the results presented by Nickel and Buballa at $T = 0$ the energetically preferred values of q are higher than our calculations indicate. This could be not significant, since another regularization scheme was used, but it should be investigated in detail. The upper end of the window is lower than their result and the

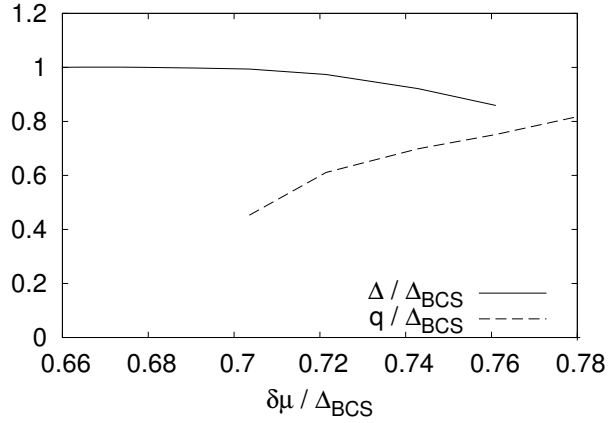


Figure 4.11.: Preferred value of the wave number $|\vec{q}|$ and the corresponding magnitude of the gap for different $\delta\mu$'s in the general one-dimensional modulated phase at $T = 0$ and $\bar{\mu} = 400$ MeV.

lower critical value $\delta\mu_1$ could in contrast be consistent with their value of $\delta\mu_2^{\text{ref}} = 0.695 \Delta_{\text{BCS}}$, but a better precision and more data will be needed to distinguish that.

The magnitude of the gap at the energetically preferred value of q agrees well with their results. Our amplitude of the gap-function remains constant below $\delta\mu_1$, whereas it is rising in the energetical Pauli-Villars regularization. For larger $\delta\mu$ the gap decreases until it vanishes after a first-order phase-transition. For non-zero temperatures the generic inhomogeneous phase seems to be favored over the Fulde-Ferrell phase, which is supported by our findings in Fig. 4.12 for $T = 0$. The order of the phase transition of the generic inhomogeneous phase to the BCS phase is second-order or very weakly first-order, which is very hard to find out numerically. The first-order phase transition to the restored phase is clearly visible, as shown in Fig. 4.12. That allows us to linearly interpolate the thermodynamic potential, where the thermodynamic potential of the restored phase was subtracted, between the last data point where the generic inhomogeneous phase is still favored and the first point, where we find that it is disfavored over the restored phase. This yields a more precise value of $\delta\mu_2$ and for zero temperature this gives $\delta\mu_2 = 0.768 \Delta_{\text{BCS}}$. Analogously this is also done for non-zero temperatures, as can be seen in Fig. 4.13. There the generic inhomogeneous phase hides the FF phase completely in the $\delta\mu - T$ -plane and undergoes a first-order phase transition to the restored phase, whereas the transition to the BCS phase is of second order.

For another average chemical potential $\bar{\mu} = 430$ MeV we calculate the wave vector and magnitude of the gap at two $\delta\mu$ values. The wave number q at $\delta\mu = 0.74 \Delta_{\text{BCS}}$ is of the order $q = 1.2 \Delta_{\text{BCS}}$ and for $\delta\mu = 0.76 \Delta_{\text{BCS}}$ it is $q = 1.5 \Delta_{\text{BCS}}$. The value almost doubles at the latter value of the chemical potential mismatch in comparison to the solution at $\bar{\mu} = 400$ MeV and for the lower mismatch the solution for the wave number is almost twice as large as for $\bar{\mu} = 400$ MeV. These high values are not understood at present and the origin of this effect remains unclear. Thus this problem must be investigated carefully. The result should be cross-checked again and compared to other predictions and known results to rule out possible uncertainties in the numerical calculations or our assumptions.

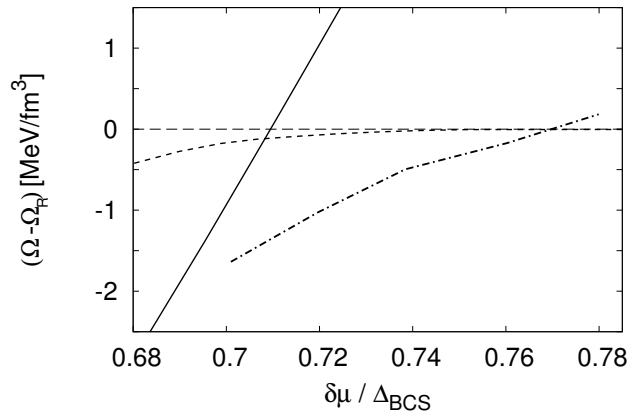


Figure 4.12.: Thermodynamic potential relative to the restored phase against the chemical potential mismatch for the BCS phase (solid), the Fulde-Ferrell phase (dashed) and the general inhomogeneous color-superconducting phase (dash-dotted) at $\bar{\mu} = 400$ MeV and $T = 0$.

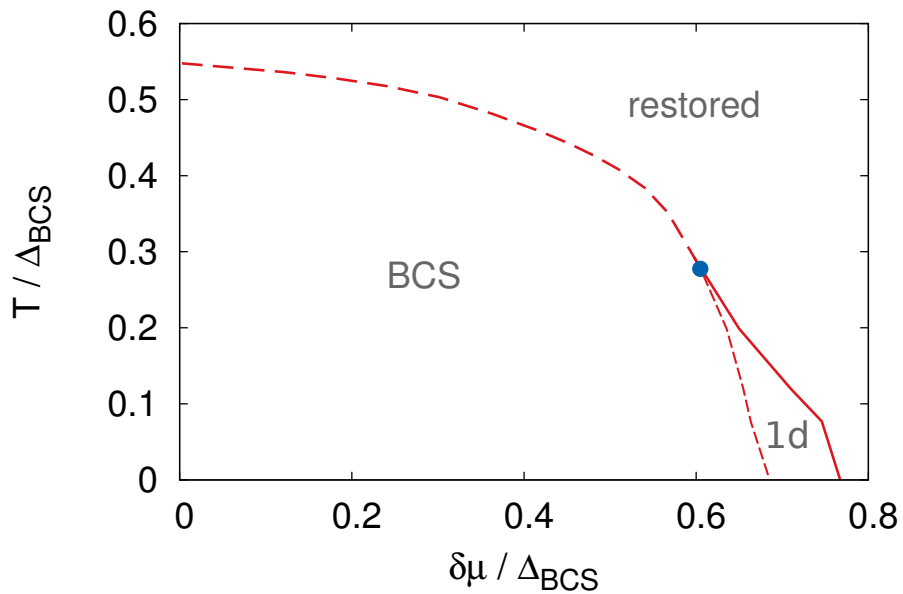


Figure 4.13.: Phase diagram for the BCS phase and generic inhomogeneous color-superconducting phase (1d) at $\bar{\mu} = 400$ MeV.

5 Conclusion and outlook

In this thesis we analysed the occurrence of inhomogeneous phases within a two-flavor Nambu–Jona-Lasinio model, studied the competition of inhomogeneous chirally broken phases with homogeneous 2SC phases for a realistic parameter set and implemented inhomogeneous phases in color-superconductivity. For the regularization of the diverging parts in the thermodynamic potential we propose to use a Pauli-Villars regularization, which does not lead to unwanted artefacts for chirally broken and color-superconducting phases. The Stefan-Boltzmann limit for high temperatures is reached in this scheme, if the temperature dependent diverging parts remain unregularized.

This regularization scheme was used to consistently study the competition of homogeneous 2SC and inhomogeneous chirally broken phases. For this we assumed that the different phases do not mix and the two quark flavors have the same chemical potential $\mu_u = \mu_d$.

The phase diagram for our standard choice of realistic parameters shows a region where an inhomogeneous window for medium to high temperatures and intermediate densities persists. The exact shape of the phase diagram is sensitive to the quark-quark coupling strength: For weaker coupling in the quark-quark channel the area, where inhomogeneous chirally broken condensates are favored, gets larger and extends to regions where formerly 2SC phases were favored. For stronger coupling the 2SC phase is favored over the inhomogeneous chiral one in most areas of the phase diagram and only a small window around the Lifshitz point remains, where inhomogeneous chiral phases are energetically preferred.

As a second part inhomogeneous color-superconducting phases were studied, which can emerge if there is a mismatch between the up and down quark's chemical potential. The existing formalism was applied to the BCS and Fulde-Ferrell phase and we extended this to finite temperatures and different average chemical potentials $\bar{\mu}$. Here it was assumed that the high density approximation holds for our case, i.e. quarks scatter only around the Fermi sphere.

The phase diagram in the $\delta\mu - T$ and for fixed $\delta\mu$ also in the $\mu - T$ plane was derived in this framework and we find that the Fulde-Ferrell phase is favored over the BCS phase for a small window in $\delta\mu$ and up to intermediate temperatures. The transition between the BCS and Fulde-Ferrell phase for varying chemical potential mismatch is of first order and the Fulde-Ferrell phase is enclosed by a second-order phase transition line to the restored phase. For the $\mu - T$ plane the Fulde-Ferrell phase is only favored for small areas at high chemical potential mismatch.

For a color-superconducting phase with generic one-dimensional modulation of the order parameter the proposed regularization scheme was modified for the numerical analysis, where the regulators were directly inserted in the Hamiltonian before diagonalizing. The $\delta\mu$ window extends in comparison to the Fulde-Ferrell phase and the generic phase is favored for a larger region. The width of the window, where the generic inhomogeneous color-superconducting phase is favored decreases with increasing temperature. Only few data-points were available for this analysis at $T \neq 0$ and the numerical slow-down due to the regularization scheme also did not allow us to derive a $\mu - T$ diagram, which could be a next step.

If the average chemical potential $\bar{\mu}$ is altered for the general inhomogeneous color-superconducting phases unexpected results were obtained in our calculations. This must be checked and an extended systematic study for our parameter dependencies should be carried out.

Additionally it is possible to study the effects of different coupling strengths in the quark-quark interaction channel for the Fulde-Ferrell and generic inhomogeneous color-superconducting phase.

For the generic inhomogeneous color-superconducting phase it would be good to find a better suited regularization scheme, which does not slow down the numerical evaluation. On the other hand the study of inhomogeneous phases could also be implemented in a renormalizable model, where the regularization artefacts do not appear.

The simultaneous occurrence of inhomogeneous chirally broken and color-superconducting phases is of interest. As a requirement the chemical potential difference between the two quark flavors also has to be introduced for (in)homogeneous chirally broken phases in our regularization scheme. This allows to compare the results for inhomogeneous chirally broken phases with the inhomogeneous 2SC phases, under the assumptions that these phases do not mix, as already done for equal chemical quark potentials $\mu_u = \mu_d$.

For future works the inclusion of chirally broken phases with a plane-wave modulation and the Fulde-Ferrell phase of color superconductivity serves as a starting point. Generic modulations will be far more complicated. For each of the inhomogeneous condensates with a plane-wave modulation of the order parameter there are known analytical solutions, which could possibly be extended for their simultaneous appearance in our model within the Pauli-Villars regularization scheme.

A Simplification of the effective Hamiltonian for inhomogeneous 2SC condensates

In chap. 4 inhomogeneous 2SC phases were considered in the NJL-model and PV-regularization. In this appendix we present selected details of the calculations for the introduced simplifications and assumptions, which were made during the evaluation of the Hamiltonian. First we show how to simplify the Hamiltonian by identifying a block-structure and as a second part we proof, that the Hamiltonian is still diagonal in the Matsubara frequencies and has the structure given in eq. (4.16).

A.1 On the Bloch theorem and Brillouin zone

The following discussion of the Bloch theorem is taken from Ref. [AM07] and will be briefly summarized for our application to inhomogeneous color-superconducting phases:

The Schrödinger equation takes a special form if the translation operator and the Hamiltonian commute: If the eigenfunctions are expanded with coefficients $\psi_k(x)$ for vector $k \in \text{B.Z.}$ the overall Schrödinger equation in momentum space can be separated in independent Schrödinger equations if the momenta fulfill

$$p_m - p_n = \pm q, \quad (\text{A.1})$$

where q is an element of the reciprocal lattice, which is present because of the assumed periodic boundary conditions.

This shows that eq. (4.16) also can be decomposed like

$$\mathcal{H} = \sum_{\vec{k} \in \text{B.Z.}} \mathcal{H}(\vec{k}) \quad (\text{A.2})$$

where only the Hamiltonian $\mathcal{H}(\vec{k})$ has to be considered independently from the others instead of the full \mathcal{H} .

Mathematically we sketch here how to derive this also in our model: One block is associated with a momentum \vec{k} of the Brillouin zone (B.Z.) and the sum over all states can be separated into a sum over the different blocks times the sum over the eigenvalues of each block

$$\sum_{\lambda} \rightarrow \sum_i \sum_{\lambda_i}, \quad (\text{A.3})$$

where λ_i are the eigenvalues of block i .

In detail this permits to rewrite the overall Hamiltonian \mathcal{H} into a direct sum of Hamiltonians associated to one block

$$\mathcal{H} = \sum_{\vec{k}_n \in \text{B.Z.}} P_{\vec{k}_n} \mathcal{H} = \sum_{\vec{k}_n \in \text{B.Z.}} \mathcal{H}(\vec{k}_n), \quad (\text{A.4})$$

where the momenta $p_{m,n}$ have a common vector k and

$$(P_{\vec{k}_n})_{\vec{p}_m, \vec{p}_n} = \sum_{\vec{q}_m, \vec{q}_n \in \text{R.L.}} \delta_{\vec{p}_m - \vec{k}_n, \vec{q}_m} \delta_{\vec{p}_n, \vec{q}_n + \vec{k}_n} \quad (\text{A.5})$$

is a projector to the block associated with \vec{k}_n . By inspecting now the resulting structure, one recognizes that only a countable number of blocks (instead of overcountable many) in the overall Hamiltonian have non-vanishing entries. Then the problem reduces to determine the eigenvalues only per block instead of the eigenvalues E_{λ} in eq. (4.17) over the whole structure.

A.2 Derivation of the effective Hamiltonian

We start with the evaluation of the euclidean action

$$S_E = \int d\tau \int d^3x \mathcal{L}(x^0 = -i\tau, \vec{x}) \quad (\text{A.6})$$

$$= \int d\tau \int d^3x \bar{\Psi}(x) S^{-1}(x) \Psi(x) + \mathcal{V}, \quad (\text{A.7})$$

neglect the potential term for now and plug in the Fourier-expanded bispinors and gap

$$\frac{1}{V} \int d\tau \int d^3x \sum_{\omega_n, \omega_m} \sum_{p_m, p_n} \bar{\Psi}_{p_m} \exp(ip_m x) S^{-1} \bar{\Psi}_{p_n} \exp(-ip_n x) \quad (\text{A.8})$$

$$= \frac{1}{V} \int d\tau \int d^3x \sum_{\omega_n, \omega_m} \sum_{p_m, p_n} \bar{\Psi}_{p_m} \exp(i(\omega_n \tau - \vec{p}_m \vec{x})) \times \\ \times \begin{pmatrix} i\cancel{\partial} + \cancel{\mu} - m & \sum_{q_k} \hat{\Delta}_{q_k} \exp(-iq_k x) \gamma_5 \\ -\sum_{q_k} \hat{\Delta}_{q_k}^* \exp(iq_k x) \gamma_5 & i\cancel{\partial} - \cancel{\mu} - m \end{pmatrix} \bar{\Psi}_{p_n} \exp(-i(\omega_n \tau - \vec{p}_n \vec{x})) \quad (\text{A.9})$$

$$= \frac{1}{V} \int d\tau \int d^3x \sum_{\omega_n, \omega_m} \sum_{p_m, p_n} \exp(i(\omega_m - \omega_n)\tau) \bar{\Psi}_{p_m} \exp(-i\vec{p}_m \vec{x}) \times \\ \times \begin{pmatrix} i\cancel{\partial} + \cancel{\mu} - m & \sum_{q_k} \hat{\Delta}_{q_k} \exp(-iq_k x) \gamma_5 \\ -\sum_{q_k} \hat{\Delta}_{q_k}^* \exp(iq_k x) \gamma_5 & i\cancel{\partial} - \cancel{\mu} - m \end{pmatrix} \bar{\Psi}_{p_n} \exp(i\vec{p}_n \vec{x}) \quad (\text{A.10})$$

$$= \frac{1}{TV} \int d^3x \sum_{\omega_n, \omega_m} \sum_{p_m, p_n} \delta_{\omega_m, \omega_n} \bar{\Psi}_{p_m} \exp(-i\vec{p}_m \vec{x}) \times \\ \times \begin{pmatrix} i\cancel{\partial} + \cancel{\mu} - m & \sum_{q_k} \hat{\Delta}_{q_k} \exp(-iq_k x) \gamma_5 \\ -\sum_{q_k} \hat{\Delta}_{q_k}^* \exp(iq_k x) \gamma_5 & i\cancel{\partial} - \cancel{\mu} - m \end{pmatrix} \bar{\Psi}_{p_n} \exp(i\vec{p}_n \vec{x}) \quad (\text{A.11})$$

$$= \frac{1}{TV} \int d^3x \sum_{\omega_n, \omega_m} \sum_{p_m, p_n} \delta_{\omega_m, \omega_n} \bar{\Psi}_{p_m} \exp(i\vec{p}_m \vec{x}) \times \\ \times \begin{pmatrix} \cancel{p}_m + \cancel{\mu} - m & \sum_{q_k} \hat{\Delta}_{q_k} \exp(-iq_k x) \gamma_5 \\ -\sum_{q_k} \hat{\Delta}_{q_k}^* \exp(iq_k x) \gamma_5 & \cancel{p}_m - \cancel{\mu} - m \end{pmatrix} \bar{\Psi}_{p_n} \exp(i\vec{p}_n \vec{x}) \quad (\text{A.12})$$

and

$$= \frac{1}{TV} \int d^3x \sum_{\omega_n, \omega_m} \sum_{P_m, P_n} \delta_{\omega_m, \omega_n} \bar{\Psi}_{P_m} \exp(-i\vec{p}_m \vec{x}) \times \begin{pmatrix} i(-i)\not{p}_m + \not{\mu} - m & \sum_{q_k} \hat{\Delta}_{q_k} \exp(-iq_k x) \gamma_5 \\ -\sum_{q_k} \hat{\Delta}_{q_k}^* \exp(iq_k x) \gamma_5 & \not{p}_m - \not{\mu} - m \end{pmatrix} \Psi_{P_n} \exp(i\vec{p}_n \vec{x}) \quad (\text{A.13})$$

$$= \frac{1}{TV} \int d^3x \sum_{\omega_n, \omega_m} \sum_{P_m, P_n} \delta_{\omega_m, \omega_n} \bar{\Psi}_{P_m} \exp(-i\vec{p}_m \vec{x}) \times \begin{pmatrix} \not{p}_m + \not{\mu} - m & \sum_{q_k} \hat{\Delta}_{q_k} \exp(-iq_k x) \gamma_5 \\ -\sum_{q_k} \hat{\Delta}_{q_k}^* \exp(iq_k x) \gamma_5 & \not{p}_m - \not{\mu} - m \end{pmatrix} \Psi_{P_n} \exp(i\vec{p}_n \vec{x}) \quad (\text{A.14})$$

$$= \frac{1}{TV} \int d^3x \sum_{\omega_n} \sum_{P_m, P_n} \bar{\Psi}_{P_m} \exp(-i\vec{p}_m \vec{x}) \times \begin{pmatrix} i\gamma^0 \omega_n - \vec{\gamma} \vec{p}_n + \not{\mu} - m & \sum_{q_k} \hat{\Delta}_{q_k} \exp(-iq_k x) \gamma_5 \\ -\sum_{q_k} \hat{\Delta}_{q_k}^* \exp(iq_k x) \gamma_5 & i\gamma^0 \omega_n - \vec{\gamma} \vec{p}_m - \not{\mu} - m \end{pmatrix} \Psi_{P_n} \exp(i\vec{p}_n \vec{x}) \quad (\text{A.15})$$

$$= \frac{1}{TV} \int d^3x \sum_{\omega_n} \sum_{P_m, P_n} \bar{\Psi}_{P_m} \exp(-i\vec{p}_m \vec{x}) \times \begin{pmatrix} i\gamma^0 \omega_n - \vec{\gamma} \vec{p}_n + \not{\mu} - m & \sum_{q_k} \hat{\Delta}_{q_k} \exp(-iq_k x) \gamma_5 \\ -\sum_{q_k} \hat{\Delta}_{q_k}^* \exp(iq_k x) \gamma_5 & i\gamma^0 \omega_n - \vec{\gamma} \vec{p}_m - \not{\mu} - m \end{pmatrix} \Psi_{P_n} \exp(i\vec{p}_n \vec{x}), \quad (\text{A.16})$$

where we used $p_m^0 = p_n^0$.

Now shifting the exponentials in the matrix and using the integral representation of the delta distribution again gives

$$= \frac{1}{TV} \sum_{\omega_n} \sum_{P_m, P_n} \int d^3x \bar{\Psi}_{P_m} \exp(-i\vec{p}_m \vec{x}) \times \begin{pmatrix} i\gamma^0 \omega_n - \vec{\gamma} \vec{p}_n + \not{\mu} - m & \sum_{q_k} \hat{\Delta}_{q_k} \exp(-iq_k x) \gamma_5 \\ -\sum_{q_k} \hat{\Delta}_{q_k}^* \exp(iq_k x) \gamma_5 & i\gamma^0 \omega_n - \vec{\gamma} \vec{p}_m - \not{\mu} - m \end{pmatrix} \Psi_{P_n} \exp(i\vec{p}_n \vec{x}) \quad (\text{A.17})$$

$$= \frac{1}{TV} V \sum_{\omega_n} \sum_{P_m, P_n} \bar{\Psi}_{P_m} \times \begin{pmatrix} i\gamma^0 \omega_n \delta_{P_m, P_n} - \vec{\gamma} \vec{p}_n \delta_{P_m, P_n} + \not{\mu} \delta_{P_m, P_n} - m \delta_{P_m, P_n} & \sum_{q_k} \hat{\Delta}_{q_k} \delta_{q_k, P_m - P_n} \gamma_5 \\ -\sum_{q_k} \hat{\Delta}_{q_k}^* \delta_{q_k, P_n - P_m} \gamma_5 & i\gamma^0 \omega_n \delta_{P_m, P_n} - \vec{\gamma} \vec{p}_m \delta_{P_m, P_n} - \not{\mu} \delta_{P_m, P_n} - m \delta_{P_m, P_n} \end{pmatrix} \Psi_{P_n}$$

which finally allows to decompose

$$S_E = \frac{1}{T} \sum_{P_m, P_n} \bar{\Psi}_{P_m} S_{P_m, P_n}^{-1} \Psi_{P_n} - \mathcal{V} \quad (\text{A.18})$$

where we defined the components of S^{-1} like in eq. (4.15). This shows that the inverse propagator is indeed diagonal in the Matsubara frequencies and

$$S_{P_m, P_n}^{-1} = \gamma^0 \left(i\omega_{P_n} - \mathcal{H}_{\vec{p}_m, \vec{p}_n} \right) \delta_{\omega_{P_m}, \omega_{P_n}} \quad (\text{A.19})$$

enables to get the effective Hamiltonian eq. (4.16).

Conventions and notation

For this thesis we use natural units where $k_B = c = \hbar := 1$ and the unit of the energy, the electron volt $[E] = \text{eV}$ was chosen as a reference and all other units are expressed in terms of this unit.

The number i is defined by $i^2 = -1$ for $i \in \mathbb{C}$.

The Feynmann slash is given by

$$\not{A} := \gamma^\mu A_\mu \quad (\text{A.20})$$

and the dagger-operator as

$$A^\dagger := \bar{A} \gamma^0, \quad (\text{A.21})$$

where γ^μ are Dirac gamma-matrices. Also we sum implicitly over same indices, where greek indices run from 0 to 3 and latin indices from 1 to 3.

The Pauli matrices are given by

$$\sigma^1 = \begin{pmatrix} 0 & 1 \\ 1 & 0 \end{pmatrix}, \sigma^2 = \begin{pmatrix} 0 & -i \\ i & 0 \end{pmatrix}, \sigma^3 = \begin{pmatrix} 1 & 0 \\ 0 & -1 \end{pmatrix}, \quad (\text{A.22})$$

and the Gell-Mann matrices by

$$\begin{aligned} \tau^1 &= \begin{pmatrix} 0 & 1 & 0 \\ 1 & 0 & 0 \\ 0 & 0 & 0 \end{pmatrix}, \tau^2 = \begin{pmatrix} 0 & -i & 0 \\ i & 0 & 0 \\ 0 & 0 & 0 \end{pmatrix}, \tau^3 = \begin{pmatrix} 1 & 0 & 0 \\ 0 & -1 & 0 \\ 0 & 0 & 0 \end{pmatrix}, \tau^4 = \begin{pmatrix} 0 & 0 & 1 \\ 0 & 0 & 0 \\ 1 & 0 & 0 \end{pmatrix}, \\ \tau^5 &= \begin{pmatrix} 0 & 0 & -i \\ 0 & 0 & 0 \\ i & 0 & 0 \end{pmatrix}, \tau^6 = \begin{pmatrix} 0 & 0 & 0 \\ 0 & 0 & 1 \\ 0 & 1 & 0 \end{pmatrix}, \tau^7 = \begin{pmatrix} 0 & 0 & 0 \\ 0 & 0 & -i \\ 0 & i & 0 \end{pmatrix}, \tau^8 = \frac{1}{\sqrt{3}} \begin{pmatrix} 1 & 0 & 0 \\ 0 & 1 & 0 \\ 0 & 0 & -2 \end{pmatrix} \end{aligned} \quad (\text{A.23})$$

obeying $\text{tr}(\tau^i \tau^j) = 2\delta^{ij}$. In the standard representation the Dirac-gamma matrices are given by

$$\gamma^i = \begin{pmatrix} 0 & \sigma^i \\ -\sigma^i & 0 \end{pmatrix}, \quad i \in \{1, 2, 3\},$$

$$\gamma^0 = \begin{pmatrix} 1_{2 \times 2} & 0 \\ 0 & -1_{2 \times 2} \end{pmatrix}$$

and

$$\gamma^5 = i\gamma^0\gamma^1\gamma^2\gamma^3,$$

all obeying $\{\gamma^\mu, \gamma^\nu\} = 2g^{\mu\nu}$, where $g^{\mu\nu}$ denotes the metric tensor $g = \text{diag}(1, -1, -1, -1)$ and $\{\cdot, \cdot\}$ the anticommutator. Other representations of the Dirac gamma-matrices can be transformed to become the standard representation and are not explicitly given here.

The special unitary group with n dimensions is given as the group of unitary $n \times n$ matrices with determinant 1 and is denoted by $\text{SU}(n)$, which is a matrix Lie group with dimension $n^2 - 1$.

Bibliography

- [ABD⁺09] Y. Aoki, S. Borsányi, S. Dürr, Z. Fodor, S. D. Katz, S. Krieg, and K. Szabo. The QCD transition temperature: results with physical masses in the continuum limit II. *J High Energy Phys.*, 6:88–+, June 2009, 0903.4155.
- [ABR01] M. Alford, J. A. Bowers, and K. Rajagopal. Crystalline color superconductivity. *Phys. Rev. D*, 63(7):074016–+, April 2001, arXiv:hep-ph/0008208.
- [AM07] N.W. Ashcroft and D.N. Mermin. *Festkörperphysik*. Oldenbourg Wissensch.Vlg, 2007.
- [ARW98] M. Alford, K. Rajagopal, and F. Wilczek. QCD at finite baryon density: Nucleon droplets and color superconductivity. *Phys. Lett. B*, 422:247–256, March 1998, arXiv:hep-ph/9711395.
- [ASRS08] M. G. Alford, A. Schmitt, K. Rajagopal, and T. Schäfer. Color superconductivity in dense quark matter. *Reviews of Modern Physics*, 80:1455–1515, October 2008, arXiv:hep-ph/0709.4635.
- [BCS57] J. Bardeen, L. N. Cooper, and J. R. Schrieffer. Theory of superconductivity. *Phys. Rev.*, 108(5):1175–1204, Dec 1957.
- [BL82] D. Bailin and A. Love. Superconductivity in quark matter. *Nucl. Phys. B*, 205(1):119 – 129, 1982.
- [Blo29] F. Bloch. Über die Quantenmechanik der Elektronen in Kristallgittern. *Zeitschrift für Physik A Hadrons and Nuclei*, 52:555–600, 1929.
- [Cha62] B. S. Chandrasekhar. A note on the maximum critical field of high-field superconductors. *App. Phys. Lett.*, 1(7), 1962.
- [Clo62] A. M. Clogston. Upper limit for the critical field in hard superconductors. *Phys. Rev. Lett.*, 9(6):266–267, Sep 1962.
- [Coh03] T. D. Cohen. Functional Integrals for QCD at Nonzero Chemical Potential and Zero Density. *Phys. Rev. Lett.*, 91(22):222001, November 2003.
- [Coo67] J. L. B. Cooper. The foundations of thermodynamics. *J. Math. Ana. Appl.*, 17(1):172 – 193, 1967.
- [CP75] J. C. Collins and M. J. Perry. Superdense matter: Neutrons or asymptotically free quarks? *Phys. Rev. Lett.*, 34(21):1353–1356, May 1975.
- [FF64] P. Fulde and R. A. Ferrell. Superconductivity in a strong spin-exchange field. *Phys. Rev.*, 135(3A):A550–A563, Aug 1964.
- [Fis06] C. S. Fischer. Infrared properties of QCD from Dyson Schwinger equations. *J. Phys. G Nucl. Partic.*, 32:253, August 2006, arXiv:hep-ph/0605173.
- [Gor59] L. P. Gor’kov. Microscopic derivation of the Ginzburg-Landau equations in the theory of superconductivity. *Sov. Phys. JETP*, 9:1364–1367, 1959.
- [Kap89] J.I. Kapusta. *Finite-temperature field theory*. Cambridge monographs on mathematical physics. Cambridge University Press, 1989.

-
- [KL04] F. Karsch and E. Laermann. Thermodynamics and in-medium hadron properties from lattice QCD. In R. C. Hwa & X.-N. Wang, editor, *Quark-Gluon Plasma*, pages 1–+, 2004, arXiv:hep-lat/0305025.
- [Kle92] S. P. Klevansky. The Nambu—Jona-Lasinio model of quantum chromodynamics. *Rev. Mod. Phys.*, 64(3):649–708, Jul 1992.
- [Nam60] Y. Nambu. Quasi-particles and gauge invariance in the theory of superconductivity. *Phys. Rev.*, 117(3):648–663, Feb 1960.
- [NB09] D. Nickel and M. Buballa. Solitonic ground states in (color) superconductivity. *Phys. Rev. D*, 79(5):054009–+, March 2009, arXiv:hep-ph/0811.2400.
- [Nic09a] D. Nickel. How Many Phases Meet at the Chiral Critical Point? *Phys. Rev. Lett.*, 103(7):072301–+, August 2009, arXiv:hep-ph/0902.1778.
- [Nic09b] D. Nickel. Inhomogeneous phases in the Nambu-Jona-Lasinio and quark-meson model. *Phys. Rev. D*, 80(7):074025–+, October 2009, arXiv:hep-ph/0906.5295.
- [NJL61a] Y. Nambu and G. Jona-Lasinio. Dynamical model of elementary particles based on an analogy with superconductivity. I. *Phys. Rev.*, 122(1):345–358, Apr 1961.
- [NJL61b] Y. Nambu and G. Jona-Lasinio. Dynamical model of elementary particles based on an analogy with superconductivity. II. *Phys. Rev.*, 124(1):246–254, Oct 1961.
- [PR99] R. D. Pisarski and D. H. Rischke. Superfluidity in a model of massless fermions coupled to scalar bosons. *Phys. Rev. D*, 60(9):094013, Oct 1999.
- [PV49] W. Pauli and F. Villars. On the invariant regularization in relativistic quantum theory. *Rev. Mod. Phys.*, 21(3):434–444, Jul 1949.
- [Red02] S. Reddy. Novel Phase at High Density and Their Role in the Structure and Evolution of Neutron Stars. *Acta Physica Polonica B*, 33:4101–+, December 2002, arXiv:nucl-th/0211045.
- [RSSV98] R. Rapp, T. Schäfer, E. Shuryak, and M. Velkovsky. Diquark bose condensates in high density matter and instantons. *Phys. Rev. Lett.*, 81(1):53–56, Jul 1998.
- [VW91] U. Vogl and W. Weise. The Nambu and Jona-Lasinio model: Its implications for hadrons and nuclei. *Prog. Part. Nucl. Phys.*, 27:195 – 272, 1991.

Danksagung

An dieser Stelle möchte ich mich bei Allen bedanken, die mich während meines Studiums und dieser Arbeit unterstützt und gefördert haben.

Insbesondere danke ich Herrn Prof. Wambach für seine Unterstützung und die Gelegenheit diese interessante Arbeit in seiner Gruppe anfertigen zu können. Desweiteren gilt besonderer Dank Herrn Dr. Buballa für die ausgezeichnete Betreuung bei dem Anfertigen dieser Master-Arbeit, die zahlreichen Kommentare und Diskussionen sowie die herausragende Unterstützung und gute Zusammenarbeit. Stefano Carignano danke ich für die andauernde Unterstützung, die zahllosen Diskussionen, die gute Zusammenarbeit und für das Bereitstellen der Daten für inhomogene chiral gebrochene Phasen.

Weiterer Dank gilt allen Mitgliedern der Arbeitsgruppe und insbesondere Zimmer "306" im Theorie-Zentrum für die vielen Diskussionen und anregenden Kommentare.

Meinen Eltern gebührt an dieser Stelle auch besonderer Dank für ihre Unterstützung, ohne die es mir nicht möglich gewesen wäre diese Arbeit zu verfassen und mein Studium durchzuführen.